PHYSICAL REVIEW D **93,** 013006 (2016)

Spontaneous *CP* violation in lepton-sector: A common origin for θ_{13}, the Dirac *CP* phase, and leptogenesis

Biswajit Karmakar* and Arunansu Sil†

Department of Physics, Indian Institute of Technology Guwahati, 781039 Assam, India

(Received 28 September 2015; published 8 January 2016)

A possible interplay between the two terms of the general type-II seesaw formula is exercised which leads to the generation of nonzero θ_{13}. The specific flavor structure of the model, guided by the $A_4 \times Z_4 \times Z_3$ symmetry and accompanied with the Standard Model singlet flavons, yields the conventional seesaw contribution to produce the tribimaximal lepton mixing which is further corrected by the presence of the $SU(2)_L$ triplet contribution to accommodate θ_{13}. We consider the *CP* symmetry to be spontaneously broken by the complex vacuum expectation value (vev) of a singlet field S. While the magnitude of its complex vev is responsible for generating θ_{13}, its phase part induces the low energy *CP* violating phase (δ) and the *CP* violation required for leptogenesis. Hence the triplet contribution, although subdominant, plays a crucial role in providing a common source for nonzero θ_{13}, δ and *CP*-violation required for leptogenesis. We find that the recent hint for δ close to $3\pi/2$ is somewhat favored in this setup though it excludes the exact equality with $3\pi/2$. We also discuss the generation of lepton asymmetry in this scenario.

DOI: 10.1103/PhysRevD.93.013006

I. INTRODUCTION

The question whether there exists an underlying principle to understand the pattern of lepton mixing, which is quite different from the quark mixing, demands the study of neutrino mass matrix as well as the charged lepton one into a deeper level. The smallness of neutrino masses can be well understood by the seesaw mechanism in a natural way. The type-I seesaw mechanism [1–4] provides the simplest possibility by extending the Standard Model (SM) with three right-handed (RH) neutrinos. An introduction of discrete symmetries into it may reveal the flavor structure of the neutrino and charged lepton mass matrix. For example, a type-I seesaw in conjugation with A_4 explains the tribimaximal lepton mixing pattern (TBM) [5] in the presence of SM singlet flavon (charged under A_4) fields which get vacuum expectation values (vev) [6–8]. However the original approach fails to accommodate the recent observation of nonzero θ_{13} [9–12]. In [13], we have shown that an extension of the Altarelli-Feruglio (AF) model [8] by one additional flavon field can be employed to have a nonzero θ_{13} consistent with the present experimental results. The setup also constrains the two Majorana phases involved in the lepton mixing matrix. The deviation of the TBM pattern is achieved through a deformation of the RH neutrino mass matrix compared to the original one. On the other hand, within the framework of a general type-II seesaw mechanism [where both RH neutrinos and $SU(2)_L$ triplet Higgs are present], light neutrino mass depends upon the comparative magnitude of the pure type-I (mediated by heavy RH neutrinos) and triplet contributions. This interplay is well studied in the literature [14–23]. In recent years keeping in mind that θ_{13} is nonzero, efforts have been given to realize leptogenesis [24–30] and linking it with θ_{13} in models based on the type-II seesaw [31].

In this paper, we focus on the generation of the light neutrino mass matrix through a type-II seesaw mechanism [32–35]. The fields content of the SM is extended with three right-handed neutrinos, one $SU(2)_L$ triplet and a set of SM singlet flavon fields. A flavor symmetry $A_4 \times Z_4 \times Z_3$ is considered. The type-II seesaw mechanism therefore consists of the conventional type-I seesaw contribution (m_ν^I) along with the triplet contribution (m_ν^{II}) to the neutrino mass matrix. Here we find the type-I contribution alone can generate the TBM mixing pattern, where the charged lepton mass matrix is a diagonal one. Then we have shown that the same flavor symmetry allows us to have a deviation from the conventional type-I contribution, triggered by the $SU(2)_L$ triplet's vev. We have found that this deviation is sufficient enough to keep θ_{13} at an acceptable level [36–38]. We mostly consider the triplet contribution to the light neutrino mass is subdominat compared to the conventional type-I contribution.

We further assume that apart from the flavons (SM singlets charged under A_4) involved, there is a A_4 singlet (as well as SM gauge singlet) field S, which gets a complex vacuum expectation value and thereby responsible for spontaneous *CP* violation[1] at high scale [47–55]. All other flavons have real vevs and all the couplings involved are

*k.biswajit@iitg.ernet.in
†asil@iitg.ernet.in

[1]Earlier it has been shown that the idea of spontaneous *CP* violation [39] can be used to solve the strong *CP* problem [40,41]. Later it has been successfully applied on models based on $SO(10)$ [42,43] and other extensions of the Standard Model [44–46].

considered to be real. It turns out that the magnitude of this complex vacuum expectation value of S is responsible for the deviation of TBM by generating the nonzero value of θ_{13} in the right ballpark. On the other hand, the phase associated with it generates the Dirac CP violating phase in the lepton sector. So in a way, the triplet contribution provides a unified source for CP violation and nonzero θ_{13}. In the lepton sector, the other possibilities where CP violation can take place involve a complex vev of Higgs triplets [56–60], or when a Higgs bidoublet (particularly in left-right models) gets complex vev [61] or in a mixed situation [62–64]. However, we will concentrate in a situation where a scalar singlet S present in the theory gets complex vev as in [48]. We have also studied the lepton asymmetry production through the decay of the heavy triplet involved. The decay of the triplet into two leptons contributes to the asymmetry where the virtual RH neutrinos are involved in the loop. This process is effective when the triplet is lighter than all the RH neutrinos. It turns out that sufficient lepton asymmetry can be generated in this way. On the other hand, if the triplet mass is heavier than the RH neutrino masses, the lightest RH neutrino may be responsible for producing lepton asymmetry where the virtual triplet is contributing in the one-loop diagram.

In [48], authors investigated a scenario where the triplet vevs are the sole contribution to the light neutrino mass and a single source of spontaneous CP violation was considered. There, it was shown that the low energy CP violating phase and the CP violation required for leptogenesis both are governed by the argument of the complex vev of that scalar field. The nonzero value of θ_{13} however followed from a perturbative deformation of the vev alignment of the flavons involved. Here in our scenario, the TBM pattern is realized by the conventional type-I contribution. Therefore in the TBM limit, θ_{13} is zero in our setup. Also there is no CP violating phase in this limit as all the flavons involved in m_ν^I are carrying real vevs, and hence no lepton asymmetry as well. Now once the triplet contribution (m_ν^{II}) is switched on, not only the θ_{13}, but also the leptonic CP violation turn out to be nonzero. For generating lepton asymmetry, two triplets were essential in [48], while we could explain the lepton asymmetry by a single triplet along with the presence of RH neutrinos. In this case, the RH neutrinos are heavier compared to the mass of the triplet involved.

TABLE I. Summary of neutrino oscillation parameters for normal and inverted neutrino mass hierarchies from the analysis of [38].

Oscillation parameters	Best fit	1σ range	3σ range
Δm^2_{21} $[10^{-5}\text{eV}^2]$	7.60	7.42–7.79	7.11–8.18
$\lvert\Delta m^2_{31}\rvert$ $[10^{-3}\text{eV}^2]$	2.48 (NH)	2.41–2.53	2.30–2.65
	2.38 (IH)	2.32–2.43	2.20–2.54
$\sin^2\theta_{12}$	0.323	0.307–0.339	0.278–0.375
$\sin^2\theta_{23}$	0.567 (NH)	0.439–0.599	0.392–0.643
	0.573 (IH)	0.530–0.598	0.403–0.640
$\sin^2\theta_{13}$	0.0234 (NH)	0.0214–0.0254	0.0177–0.0294
	0.0240 (IH)	0.0221–0.0259	0.0183–0.0297

The paper is organized as follows. In Sec. II, we provide the status of the neutrino mixing and the mass squared differences. Then in Sec. III, we describe the setup of the model followed by constraining the parameter space of the framework from neutrino masses and mixing in Sec. IV. In Sec. V, we describe how one can obtain lepton asymmetry out of this construction. Finally we conclude in Sec. VI.

II. STATUS OF NEUTRINO MASSES AND MIXING

Here we summarize the neutrino mixing parameters and their present status. The neutrino mass matrix m_ν, in general, can be diagonalized by the U_{PMNS} matrix (in the basis where charged lepton mass matrix is diagonal) as $m_\nu = U^*_{PMNS}\text{diag}(m_1, m_2, m_3)U^\dagger_{PMNS}$, where m_1, m_2, m_3 are the real mass eigenvalues for light neutrinos. The standard parametrization of the U_{PMNS} matrix [65] is given by

$$U_{PMNS} = \begin{pmatrix} c_{12}c_{13} & s_{12}c_{13} & s_{13}e^{-i\delta} \\ -s_{12}c_{23} - c_{12}s_{13}s_{23}e^{i\delta} & c_{12}c_{23} - s_{12}s_{13}s_{23}e^{i\delta} & c_{13}s_{23} \\ s_{12}s_{23} - c_{12}s_{13}c_{23}e^{i\delta} & -c_{12}s_{23} - s_{12}s_{13}c_{23}e^{i\delta} & c_{13}c_{23} \end{pmatrix} \begin{pmatrix} 1 & 0 & 0 \\ 0 & e^{i\alpha_{21}/2} & 0 \\ 0 & 0 & e^{i\alpha_{31}/2} \end{pmatrix}, \tag{2.1}$$

where $c_{ij} = \cos\theta_{ij}$, $s_{ij} = \sin\theta_{ij}$, the angles $\theta_{ij} = [0, \pi/2]$, $\delta = [0, 2\pi]$ is the CP-violating Dirac phase while α_{21} and α_{31} are the two CP-violating Majorana phases. The mixing angles θ_{12}, θ_{23} and the two mass-squared differences $\Delta m^2_{12}(\equiv m_2^2 - m_1^2)$, $\Delta m^2_{31}(\equiv m_3^2 - m_1^2)$ have been well measured at several neutrino oscillation experiments [66]. Recently the other mixing angle θ_{13} is also reported to be of sizable magnitude [9–12]. Very recently, we start to get a hint for the nonzero Dirac CP phase [12,36–38]. From the updated global analysis [38] involving all the data from neutrino experiments, the 1σ and 3σ ranges of mixing angles and the mass-squared differences are mentioned (NH and IH stand for the normal and inverted mass hierarchies respectively) in Table I. The result by Planck [67] from the analysis of cosmic microwave background (CMB) also sets an upper limit on the sum of the three neutrino masses as given by, $\Sigma_i m_{\nu_i} < 0.23$ eV. The result from neutrinoless double beta decay by KamLAND-Zen

[68] and EXO-200 [69] indicates a limit on the effective neutrino mass parameter $|m_{ee}|$ as, $|m_{ee}| < (0.14\text{–}0.28)$ eV at 90% C.L. and $|m_{ee}| < (0.19\text{–}0.45)$ eV at 90% C.L. respectively.

III. THE MODEL

Our starting point is the conventional type-I seesaw mechanism to explain the smallness of light neutrino masses which further predicts a tribimaximal mixing (TBM) pattern in the lepton sector. For this part, we use the original AF model [8] by introducing a discrete A_4 symmetry and A_4 triplet flavon fields ϕ_S, ϕ_T along with a singlet ξ field. Of course three right-handed neutrinos (N_R) are also incorporated. In addition, we include a $SU(2)_L$ triplet field (Δ) with hypercharge unity, the vev of which produces an additional contribution (hereafter called the triplet contribution) to the light neutrino mass. So our setup basically involves a general type-II seesaw,

$$m_\nu = m_\nu^{II} + m_\nu^{I} = m_\nu^{II} - m_D^T M_R^{-1} m_D, \tag{3.1}$$

where m_ν^I is the typical type-I term and m_ν^{II} is the triplet contribution. To realize both, the relevant Lagrangian for generation of m_ν can be written as

$$-\mathcal{L} = Y_D \bar{L}\tilde{H} N_R + \frac{1}{2} M_R \overline{N_R^c} N_R + (Y_\Delta)_{ij} L_i^T C \Delta L_j, \tag{3.2}$$

so that $m_\nu^{II} = 2Y_\Delta u_\Delta$ and $m_D = Y_D v$, where u_Δ and v are the vevs of the triplet Δ and SM Higgs doublet (H) respectively. Y_D and Y_Δ correspond to the Yukawa matrices for the Dirac mass and triplet terms respectively, the flavor structure of which are solely determined by the discrete symmetries imposed on the fields involved in the model. M_R is the Majorana mass of the RH neutrinos. In the following subsection, we discuss in detail how the flavor structure of Y_D, Y_Δ and M_R are generated with the flavon fields. A discrete symmetry $Z_4 \times Z_3$ is also present in our model and two other SM singlet fields ξ' and S are introduced. These additional fields and the discrete symmetries considered play a crucial role in realizing a typical structure of the triplet contribution to the light neutrino mass matrix as we will see below. Among all these scalar fields present, only the S field is assumed to have a complex vev while all other vevs are real. The framework is based on the SM gauge group extended with the $A_4 \times Z_4 \times Z_3$ symmetry. The field contents and charges under the symmetries imposed are provided in Table II.

With the above fields content, the charged lepton Lagrangian is described by

$$\mathcal{L}_l = \frac{y_e}{\Lambda}(\bar{L}\phi_T) H e_R + \frac{y_\mu}{\Lambda}(\bar{L}\phi_T)' H \mu_R + \frac{y_\tau}{\Lambda}(\bar{L}\phi_T)'' H \tau_R, \tag{3.3}$$

TABLE II. Fields content and transformation properties under the symmetries imposed on the model.

Field	e_R	μ_R	τ_R	L	N_R	H	Δ	ϕ_S	ϕ_T	ξ	ξ'	S
A_4	1	$1''$	$1'$	3	3	1	1	3	3	1	$1'$	1
Z_4	-1	-1	-1	i	i	1	$-i$	-1	$-i$	-1	i	-1
Z_3	ω	ω	ω	ω	ω	1	ω^2	ω	1	ω	ω^2	1

to the leading order, where Λ is the cutoff scale of the theory and y_e, y_μ and y_τ are the respective coupling constants. Terms in the first parentheses represent products of two A_4 triplets, which further contracts with A_4 singlets 1, $1''$ and $1'$ corresponding to e_R, μ_R and τ_R respectively to make a true singlet under A_4. Once the flavons ϕ_S and ϕ_T get the vevs along a suitable direction as (u_S, u_S, u_S) and $(u_T, 0, 0)$ respectively,[2] it leads to a diagonal mass matrix for charged leptons, once the Higgs vev v is inserted. Below we will first summarize how the TBM mixing is achieved followed by the triplet contribution in the next subsection. The requirement of introducing SM singlet fields will be explained subsequently while discussing the flavor structure of neutrino mass matrix in detail.

A. Type-I seesaw and tribimaximal mixing

The relevant Lagrangian for the type-I seesaw in the neutrino sector is given by

$$\mathcal{L}_\mathcal{I} = y \bar{L}\tilde{H} N_R + x_A \xi \overline{N_R^c} N_R + x_B \phi_S \overline{N_R^c} N_R, \tag{3.4}$$

where y, x_A and x_B are the coupling constants. After the ξ and ϕ_S fields get vevs and the electroweak vev v is included, it yields the following flavor structure for Dirac (m_D) and Majorana (M_R) mass matrices:

$$m_D = Y_D v = yv \begin{pmatrix} 1 & 0 & 0 \\ 0 & 0 & 1 \\ 0 & 1 & 0 \end{pmatrix} \quad \text{and}$$
$$M_R = \begin{pmatrix} a + 2b/3 & -b/3 & -b/3 \\ -b/3 & 2b/3 & a - b/3 \\ -b/3 & a - b/3 & 2b/3 \end{pmatrix}, \tag{3.5}$$

with $a = 2x_A\langle\xi\rangle = 2x_A u_\xi$, $b = 2x_B u_S$. The A_4 multiplication rules that result to this flavor structure can be found in [13]. Therefore the contribution toward light neutrino mass that results from the type-I seesaw mechanism is found to be

[2]The typical vev alignments of ϕ_S and ϕ_T are assumed here. We expect the minimization of the potential involving ϕ_S and ϕ_T can produce this by proper tuning of the parameters involved in the potential. However the very details of it are beyond the scope of this paper.

$$m_\nu^I = -m_D^T M_R^{-1} m_D = -v^2 y^2 \begin{pmatrix} \frac{3a+b}{3a(a+b)} & \frac{b}{3a(a+b)} & \frac{b}{3a(a+b)} \\ \frac{b}{3a(a+b)} & -\frac{b(2a+b)}{3a(a^2-b^2)} & \frac{3a^2+ab-b^2}{3a(a^2-b^2)} \\ \frac{b}{3a(a+b)} & \frac{3a^2+ab-b^2}{3a(a^2-b^2)} & -\frac{b(2a+b)}{3a(a^2-b^2)} \end{pmatrix}. \tag{3.6}$$

Now, we introduce two parameters $\alpha = b/a$ and $k = v^2y^2/a$ which are real and positive as they are part of the type-I contribution only. Therefore, Eq. (3.6) now takes the form

$$m_\nu^I = -k \begin{pmatrix} \frac{3+\alpha}{3(1+\alpha)} & \frac{\alpha}{3(1+\alpha)} & \frac{\alpha}{3(1+\alpha)} \\ \frac{\alpha}{3(1+\alpha)} & -\frac{\alpha(2+\alpha)}{3(1-\alpha^2)} & \frac{3+\alpha-\alpha^2}{3(1-\alpha^2)} \\ \frac{\alpha}{3(1+\alpha)} & \frac{3+\alpha-\alpha^2}{3(1-\alpha^2)} & -\frac{\alpha(2+\alpha)}{3(1-\alpha^2)} \end{pmatrix}. \tag{3.7}$$

Note that this form of m_ν^I indicates that the corresponding diagonalizing matrix would be nothing but the TBM mixing matrix of the form [5]

$$U_{TB} = \begin{pmatrix} \sqrt{\frac{2}{3}} & \frac{1}{\sqrt{3}} & 0 \\ -\frac{1}{\sqrt{6}} & \frac{1}{\sqrt{3}} & -\frac{1}{\sqrt{2}} \\ -\frac{1}{\sqrt{6}} & \frac{1}{\sqrt{3}} & \frac{1}{\sqrt{2}} \end{pmatrix}. \tag{3.8}$$

As a characteristic of typical A_4 generated structure, the RH neutrinos mass matrix is as well diagonalized by the U_{TB}. In order to achieve the real and positive mass eigenvalues, the corresponding rotation U_R is provided on M_R as $U_R^T M_R U_R = M_R^{\rm diag} = {\rm diag}(a+b, a, a-b)$ with $U_R = U_{TB}{\rm diag}(1, 1, e^{-i\pi/2})$ once $a > b$ is considered. On the other hand for $a < b$; through $U_R = U_{TB}$ itself, the real and positive eigenvalues of M_R [$M_R^{\rm diag} = {\rm diag}(a+b, a, b-a)$] can be obtained. This would be useful when we will consider the decay of the RH neutrinos for leptogenesis in Sec. V.

B. Triplet contribution and type-II seesaw

The leading order Lagrangian invariant under the symmetries imposed, that describes the triplet contribution to the light neutrino mass matrix (m_ν^{II}), is given by

$$\mathcal{L}_{II} = \frac{1}{\Lambda^2} \Delta L^T L (x_1 S + x_1' S^*) \xi', \tag{3.9}$$

where x_1 and x_1' are the couplings involved. Here ξ' develops a vev $u_{\xi'}$ and the singlet S is having a complex vev $\langle S \rangle = v_S e^{i\alpha_S}$. As we have mentioned before, the vev of S provides the unique source of CP violation as all other vevs and couplings are assumed to be real. CP is therefore assumed to be conserved in all the terms involved in the Lagrangian. Similar to [48], CP is spontaneously broken by the complex vev of the S field. After plugging all these vevs, the above Lagrangian in Eq. (3.9) contributes to the following Yukawa matrix for the triplet Δ as given by

$$Y_\Delta = h \begin{pmatrix} 0 & 0 & 1 \\ 0 & 1 & 0 \\ 1 & 0 & 0 \end{pmatrix}, \qquad h = \frac{1}{\Lambda^2} u_{\xi'} v_S (x_1 e^{i\alpha_S} + x_1' e^{-i\alpha_S}). \tag{3.10}$$

This specific structure follows from the A_4 charge assignments of various fields present in Eq. (3.9) and is instrumental in providing nonzero θ_{13} as we will see shortly.

Before discussing the vev of the Δ field, let us describe the complete scalar potential V, including the triplet Δ obeying the symmetries imposed, is given by

$$V = V_S + V_H + V_\Delta + V_{SH} + V_{S\Delta} + V_{\Delta H}, \tag{3.11}$$

where

$$\begin{aligned} V_S &= \mu_S^2 (S^2 + S^{*2}) + m_S^2 S^* S + \lambda_1 (S^4 + S^{*4}) \\ &\quad + \lambda_2 S^* S (S^2 + S^{*2}) + \lambda_3 (S^* S)^2, \\ V_H &= m_H^2 H^\dagger H + \lambda_4 (H^\dagger H)^2, \\ V_\Delta &= M_\Delta^2 {\rm Tr}(\Delta^\dagger \Delta) + \lambda_5 [{\rm Tr}(\Delta^\dagger \Delta)]^2, \\ V_{SH} &= \lambda_6 (S^* S) H^\dagger H + \lambda_7 (S^2 + S^{*2})(H^\dagger H), \\ V_{S\Delta} &= {\rm Tr}(\Delta^\dagger \Delta)[\lambda_8 (S^2 + S^{*2}) + \lambda_9 S^* S], \\ V_{\Delta H} &= \lambda_{10} (H^\dagger H) {\rm Tr}(\Delta^\dagger \Delta) + \lambda_{11} (H^\dagger \Delta^\dagger \Delta H) \\ &\quad + \left(-\frac{\mu}{\Lambda} \tilde{H}^T \Delta \tilde{H} \phi_S \phi_T + {\rm H.c.} \right). \end{aligned} \tag{3.12}$$

The above potential contains several dimensionful (denoted by μ_S, $m_{S,H}$, M_Δ) and dimensionless parameters (as $\lambda_{i=1,2,\ldots,11}$ and μ), which are all considered to be real. Similar to [48], here also it can be shown that the S field gets a complex vev for a choice of parameters involved in V_S as $m_S^2 < 0$, $\mu_S \simeq 0$ and $\lambda_3 > 2\lambda_1 > 0$. However contrary to [48], here we have only a single triplet field Δ. Once the ϕ_S, ϕ_T get vevs, the last term of $V_{\Delta H}$ results into an effective ΔHH interaction which would be important for leptogenesis. The vev of the triplet Δ is obtained by minimizing the relevant terms[3] from V after plugging the vevs of the flavons and is given by

[3]We consider couplings $\lambda_{8,9} \ll 1$.

$$\langle \Delta^0 \rangle \equiv u_\Delta = \eta \frac{v^2}{M_\Delta^2} \quad \text{and} \quad \eta = \frac{\mu}{\Lambda} u_S u_T. \tag{3.13}$$

Using Eqs. (3.10) and (3.13), the triplet contribution to the light neutrino mass matrix follows from the Lagrangian $\mathcal{L}_{\mathcal{II}}$ as

$$m_\nu^{II} = \begin{pmatrix} 0 & 0 & d \\ 0 & d & 0 \\ d & 0 & 0 \end{pmatrix}, \tag{3.14}$$

where

$$d = 2hu_\Delta = 2h\eta \frac{v^2}{M_\Delta^2}. \tag{3.15}$$

Note that only the triplet contribution (d) involves the phase due to the involvement of $\langle S \rangle$ in h, while the entire type-I contribution m_ν^I remains real. Therefore the term d serves as the unique source of generating all the CP-violating phases involved in neutrino as well as in lepton mixing. This will be clear once we discuss the neutrino mixing in the subsequent section. Now we can write down the entire contribution to the light neutrino mass as

$$\begin{aligned} m_\nu &= m_\nu^I + m_\nu^{II} \\ &= -k \begin{pmatrix} \frac{3+\alpha}{3(1+\alpha)} & \frac{\alpha}{3(1+\alpha)} & \frac{\alpha}{3(1+\alpha)} \\ \frac{\alpha}{3(1+\alpha)} & -\frac{\alpha(2+\alpha)}{3(1-\alpha^2)} & \frac{3+\alpha-\alpha^2}{3(1-\alpha^2)} \\ \frac{\alpha}{3(1+\alpha)} & \frac{3+\alpha-\alpha^2}{3(1-\alpha^2)} & -\frac{\alpha(2+\alpha)}{3(1-\alpha^2)} \end{pmatrix} \\ &\quad + \begin{pmatrix} 0 & 0 & d \\ 0 & d & 0 \\ d & 0 & 0 \end{pmatrix}. \end{aligned} \tag{3.16}$$

IV. CONSTRAINING PARAMETERS FROM NEUTRINO MIXING

In this section, we discuss how the neutrino masses and mixing can be obtained from the m_ν mentioned above. Keeping in mind that m_ν^I can be diagonalized by U_{TB}, we first perform a rotation by U_{TB} on the explicit form of the light neutrino mass matrix obtained in Eq. (3.16) and the rotated m_ν is found to be

$$m_\nu' = U_{TB}^T m_\nu U_{TB} = \begin{pmatrix} -\frac{d}{2} - \frac{k}{(1+\alpha)} & 0 & \frac{\sqrt{3}d}{2} \\ 0 & d-k & 0 \\ \frac{\sqrt{3}d}{2} & 0 & \frac{d}{2} + \frac{k}{(1-\alpha)} \end{pmatrix}. \tag{4.1}$$

We note that a further rotation by U_1 (another unitary matrix) in the 13 plane in required to diagonalize the light neutrino mass matrix, $U_1^T m_\nu' U_1 = m_\nu^{\text{diag}}$. With a form of U_1 as

$$U_1 = \begin{pmatrix} \cos\theta & 0 & \sin\theta e^{-i\psi} \\ 0 & 1 & 0 \\ -\sin\theta e^{i\psi} & 0 & \cos\theta \end{pmatrix}, \tag{4.2}$$

we have $(U_{TB}U_1)^T m_\nu U_{TB} U_1 = \text{diag}(m_1 e^{i\gamma_1}, m_2 e^{i\gamma_2}, m_3 e^{i\gamma_3})$, where $m_{i=1,2,3}$ are the real and positive eigenvalues and $\gamma_{i=1,2,3}$ are the phases associated to these mass eigenvalues. We can therefore extract the neutrino mixing matrix U_ν as

$$\begin{aligned} U_\nu &= U_{TB} U_1 U_m \\ &= \begin{pmatrix} \sqrt{\frac{2}{3}}\cos\theta & \frac{1}{\sqrt{3}} & \sqrt{\frac{2}{3}} e^{-i\psi}\sin\theta \\ -\frac{\cos\theta}{\sqrt{6}} + \frac{e^{i\psi}\sin\theta}{\sqrt{2}} & \frac{1}{\sqrt{3}} & -\frac{\cos\theta}{\sqrt{2}} - \frac{e^{-i\psi}\sin\theta}{\sqrt{6}} \\ -\frac{\cos\theta}{\sqrt{6}} - \frac{e^{i\psi}\sin\theta}{\sqrt{2}} & \frac{1}{\sqrt{3}} & \frac{\cos\theta}{\sqrt{2}} - \frac{e^{-i\psi}\sin\theta}{\sqrt{6}} \end{pmatrix} U_m, \end{aligned} \tag{4.3}$$

where $U_m = \text{diag}(1, e^{i\alpha_{21}/2}, e^{i\alpha_{31}/2})$ is the Majorana phase matrix with $\alpha_{21} = (\gamma_1 - \gamma_2)$ and $\alpha_{31} = (\gamma_1 - \gamma_3)$, one common phase being irrelevant. As the charged lepton mass matrix is a diagonal one, we can now compare this U_ν with the standard parametrization of lepton mixing matrix U_{PMNS}. The U_{PMNS} is therefore given by $U_{PMNS} = U_P U_\nu$, where we need to multiply the U_ν matrix by a diagonal phase matrix U_P [70] from left as given by

$$U_P = \text{diag}\left(1, 1 + \frac{i\sin\psi}{\cos\psi + \sqrt{3}\cot\theta}, 1 + \frac{i\sin\psi}{\cos\psi - \sqrt{3}\cot\theta}\right), \tag{4.4}$$

so that the U_{PMNS} excluding the Majorana phase matrix can take the standard form where 23 and 33 elements are real as in Eq. (2.1). Hence we obtain the usual (in A_4 models) correlation [71] between the angles and CP violating Dirac phase δ as given by

$$\sin\theta_{13} = \sqrt{\frac{2}{3}}|\sin\theta|, \quad \sin^2\theta_{12} = \frac{1}{3(1-\sin^2\theta_{13})}, \tag{4.5}$$

$$\sin^2\theta_{23} = \frac{1}{2} + \frac{1}{\sqrt{2}}\sin\theta_{13}\cos\delta, \quad \delta = \arg[(U_1)_{13}]. \tag{4.6}$$

The angle θ and phase ψ associated with U_1 can now be linked with the parameters involved in m_ν. For this we first rewrite the triplet contribution d as $d = |d|e^{i\phi_d}$ and define a parameter $\beta = |d|/k$ (hence β is real). This parameter indicates the relative size of the triplet contribution to the type-I contribution when $\alpha \leq 1$. As U_1 diagonalizes the m_ν' matrix, after some involved algebra, we finally get

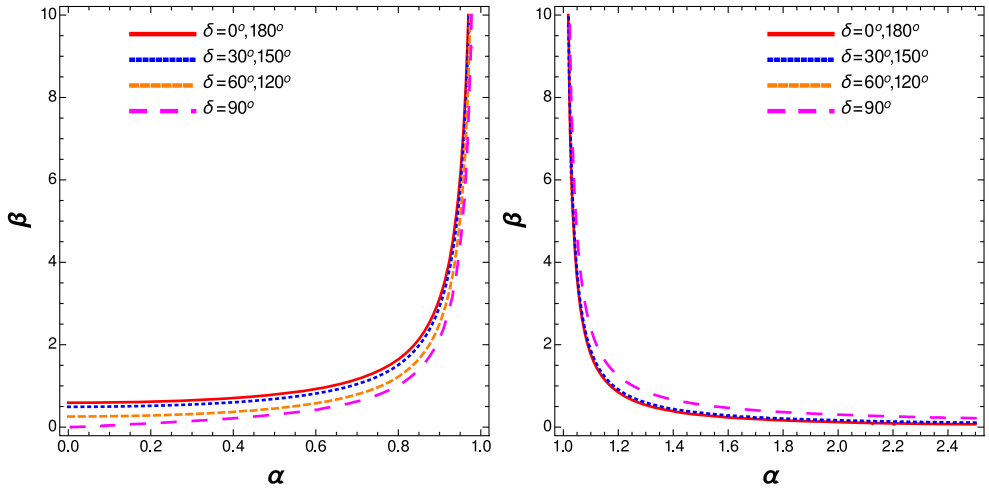

FIG. 1. Contour plots for $\sin^2\theta_{13} = 0.0234$ in the α-β plane for various choices of δ as indicated inside the figure. The left panel is for (A) $\alpha < 1$ and the right panel is with (B) $\alpha > 1$.

$$\tan 2\theta = \frac{\sqrt{3}}{\alpha}\frac{[1-(1-\alpha^2)\cos^2\phi_d]^{1/2}}{\frac{2}{\beta(1-\alpha^2)}+\cos\phi_d} \quad \text{and}$$
$$\tan\psi = (\tan\phi_d)/\alpha. \tag{4.7}$$

$\sin\theta$ may take positive or negative value depending on the choices of α, β as evident from the first relation in Eq. (4.7). For $\sin\theta > 0$, we find $\delta = \psi$ using $\delta = \arg[(U_1)_{13}$ and the second relation of Eq. (4.7).On the other hand for $\sin\theta < 0$; δ and ψ are related by $\delta = \psi \pm \pi$. Therefore in both these cases we obtain $\tan\psi = \tan\delta$ and hence

$$\tan\delta = (\tan\phi_d)/\alpha. \tag{4.8}$$

In our setup, the source of this CP-violating Dirac phase δ is through the phase α_S associated with $\langle S\rangle$. Note that $\tan\delta$ is related with $\tan\phi_d$ and α as seen from Eq. (4.8). Now from the relation $d = |d|e^{i\phi_d}$ and using Eqs. (3.10) and (3.15), we obtain ϕ_d satisfying

$$\tan\phi_d = \frac{(x_1 - x_1')}{(x_1 + x_1')}\tan\alpha_S, \tag{4.9}$$

where x_1 and x_1' are the coupling involved in Eq. (3.9).

As seen from Eqs. (4.5) and (4.7), we conclude that the U_{PMNS} parameters θ_{13} and δ depend on the model parameters α, β and ϕ_d. Note that we expect terms a and b ($\alpha = b/a$) to be of similar order of magnitude as both originated from the tree level Lagrangian [see Eqs. (3.4) and (3.5)]. We categorize $\alpha < 1$ as case A, while $\alpha > 1$ is with case B. The other parameter β basically represents the relative order of magnitude between the triplet contribution ($|d|$) and the type-I contribution (v^2y^2/a). Our framework produces the TBM mixing pattern to be generated solely by type-I seesaw and triplet contribution is present mainly to correct for the angle θ_{13} which is small compared to the other mixing angles. Therefore we consider that the triplet contribution is preferably the subdominant or at most comparable one. Therefore we expect the parameter β to be less than one. Although we discuss what happens when $\beta > 1$ in some cases, we will restrict ourselves with $\beta < 1$ for the most of the analyses involved later in this paper. In Fig. 1 (left panel), we study the variation of α and β in order to achieve the best fit value of $\sin^2\theta_{13} = 0.0234$ [38] while different values of δ are considered. In producing these plots, we have replaced the ϕ_d dependence in terms of α and δ by employing the second equation in Eq. (4.7) as $\psi = \delta$. Similarly in the right panel of Fig. 1, contour plots for $\sin^2\theta_{13} = 0.0234$ are depicted for $\alpha > 1$ with different values of δ. We find a typical contour plot for $\sin^2\theta_{13}$ with a specific δ value coincides with the one with other δ values obtained from $|\pi - \delta|$. For example, one particular contour plot for $\delta = 30°$ is repeated for $\delta = 150°$, $210°$, $330°$.

Diagonalizing m_ν' in Eq. (4.1), the light neutrino masses turn out to be

$$m_1 = k\left[\left(\frac{\alpha}{\pm(1-\alpha^2)} - \frac{p}{k}\right)^2 + \left(\frac{q}{k}\right)^2\right]^{1/2}, \tag{4.10}$$

$$m_2 = k[1+\beta^2 - 2\beta\cos\phi_d]^{1/2}, \tag{4.11}$$

$$m_3 = k\left[\left(\frac{\alpha}{\pm(1-\alpha^2)} + \frac{p}{k}\right)^2 + \left(\frac{q}{k}\right)^2\right]^{1/2}, \tag{4.12}$$

where p and q are defined as

$$\left(\frac{p}{k}\right)^2 = \frac{1}{2}\left(\frac{A}{k^2} + \sqrt{\frac{A^2}{k^4}+\frac{B^2}{k^4}}\right),$$
$$\left(\frac{q}{k}\right)^2 = \frac{1}{2}\left(-\frac{A}{k^2} + \sqrt{\frac{A^2}{k^4}+\frac{B^2}{k^4}}\right); \tag{4.13}$$

$$\frac{A}{k^2} = \beta^2\cos 2\phi_d + \beta\frac{\cos\phi_d}{1-\alpha^2} + \frac{1}{(1-\alpha^2)^2},$$
$$\frac{B}{k^2} = \beta^2\sin 2\phi_d + \beta\frac{\sin\phi_d}{1-\alpha^2}. \tag{4.14}$$

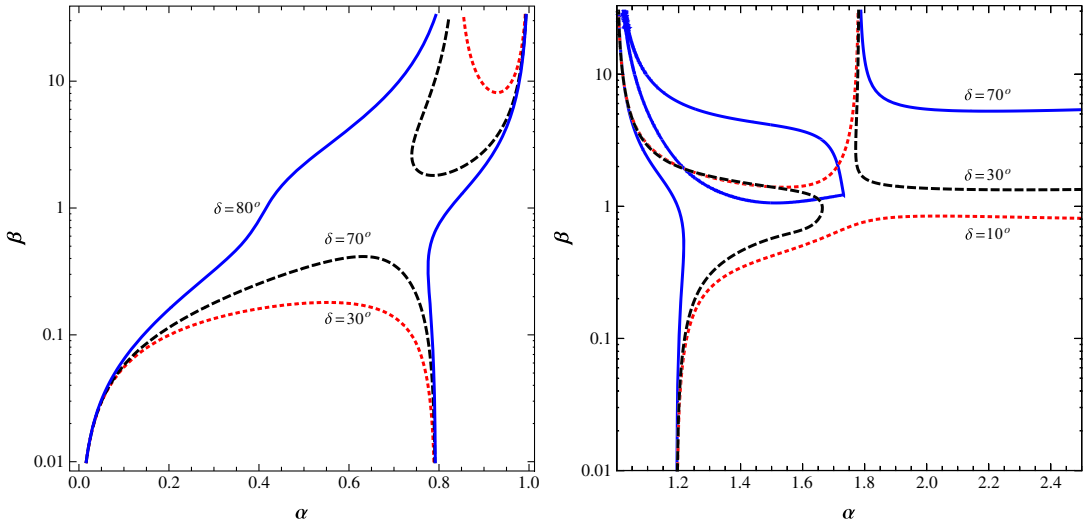

FIG. 2. Contour plots for $r = 0.03$ are shown in the α-β plane for various choices of δ. Here, in the left panel (with $\alpha < 1$, case A) red (dotted), black (dashed) and blue (continuous) lines represent $\delta = 30°$, 70° and 80° respectively. Similar contours are present for $|\pi - \delta|$ values of the *CP* violating Dirac phase. In the right panel (with $\alpha > 1$, case B) red (dotted), black (dashed) and blue (continuous) lines represent $\delta = 10°$, 30° and 70° respectively.

The "+" sign in the expression of m_1 and m_3 is for $\alpha < 1$ (case A) where the "−" sign is associated with $\alpha > 1$ (case B). The Majorana phases in U_m [see Eq. (4.3)] are found to be

$$\alpha_{21} = \tan^{-1}\left[\frac{q/k}{p/k \pm \frac{\alpha}{(\alpha^2-1)}}\right] - \tan^{-1}\left[\frac{\beta \sin\phi_d}{\beta\cos\phi_d - 1}\right], \quad (4.15)$$

$$\alpha_{31} = \pi + \tan^{-1}\left[\frac{q/k}{p/k \pm \frac{\alpha}{(\alpha^2-1)}}\right] - \tan^{-1}\left[\frac{q/k}{p/k \pm \frac{\alpha}{(1-\alpha^2)}}\right]. \quad (4.16)$$

Note that the redefined parameters p/k and q/k are functions of α, β and ϕ_d, while the mass eigenvalues m_i, depend on k as well.

The parameters α, β and ϕ_d can now be constrained by the neutrino oscillation data. To have a more concrete discussion, we consider the ratio, r, defined by $r = \frac{\Delta m^2_\odot}{|\Delta m^2_{atm}|}$, with $\Delta m^2_\odot \equiv \Delta m^2_{21} = m_2^2 - m_1^2$ and $|\Delta m^2_{atm}| \equiv \Delta m^2_{31} = m_3^3 - m_1^2$ considering normal hierarchy. Following [38], the best fit values of $\Delta m^2_\odot = 7.6 \times 10^{-5}$ eV^2 and $|\Delta m^2_{atm}| = 2.48 \times 10^{-3}$ eV^2 are used for our analysis. Using Eqs. (4.10)–(4.12), we have an expression for r as

$$r = \frac{\pm(1-\alpha^2)}{4\alpha}\frac{k}{p}\left[1 + \beta^2 - 2\beta\cos\phi_d - \left(\frac{\alpha}{\pm(1-\alpha^2)} - \frac{p}{k}\right)^2 - \left(\frac{q}{k}\right)^2\right]. \quad (4.17)$$

Here also, "+" corresponds to case A (i.e., with $\alpha < 1$) and "−" is for case B (i.e., when $\alpha > 1$). Interestingly we note that r depends on α, β and ϕ_d. Therefore using this expression of r, we can now have a contour plot for $r = 0.03$ [65] in terms of α and β for specific choices of δ as we can replace the ϕ_d dependence in terms of α and δ through Eq. (4.8). For $\alpha < 1$, this is shown in Fig. 2 (left panel) and a similar plot is made for $\alpha > 1$ in the right panel. Although we argue that it is more natural to consider β to be less than one, in this plot we allow larger values of β as a completeness. With this, for $\alpha < 1$ (case A) we see the appearance of two separate contours of $r = 0.03$ with $\delta = 30°$, one is for $\beta < 1$ and the other corresponds to $\beta > 1$. Similar plots are obtained for $\delta = 70°$ as well. However these isolated contours become a connected one once the value of δ increases, e.g., at $\delta = 80°$, it is shown in Fig. 2 (left panel). A similar pattern follows in case of the $\alpha > 1$ case. Below we discuss the predictions of our model for case A (with $\alpha < 1$) and case B ($\alpha > 1$) separately.

A. Results for case A

Note that we need to satisfy both the $\sin^2\theta_{13}$ as well as the value of r obtained from the neutrino oscillation experiments. For this reason, if we consider the two contour plots (one for $r = 0.03$ and the other for $\sin^2\theta_{13} = 0.0234$) together, then their intersection [denoted by (α, β)] should indicate a simultaneous satisfaction of these experimental data for a specific choice of δ. This is exercised in Fig. 3. In the left panel of Fig. 3, contour plots of r and $\sin^2\theta_{13}$ are drawn in terms of α and β for two choices of $\delta = 20°$ and 40°. We find that there is no such solution for (α, β) which satisfies both r and $\sin^2\theta_{13}$ with α, $\beta \lesssim 1$ in these cases. However there exists a solution for α very close to one with a pretty large value of β as mentioned in Table III. This

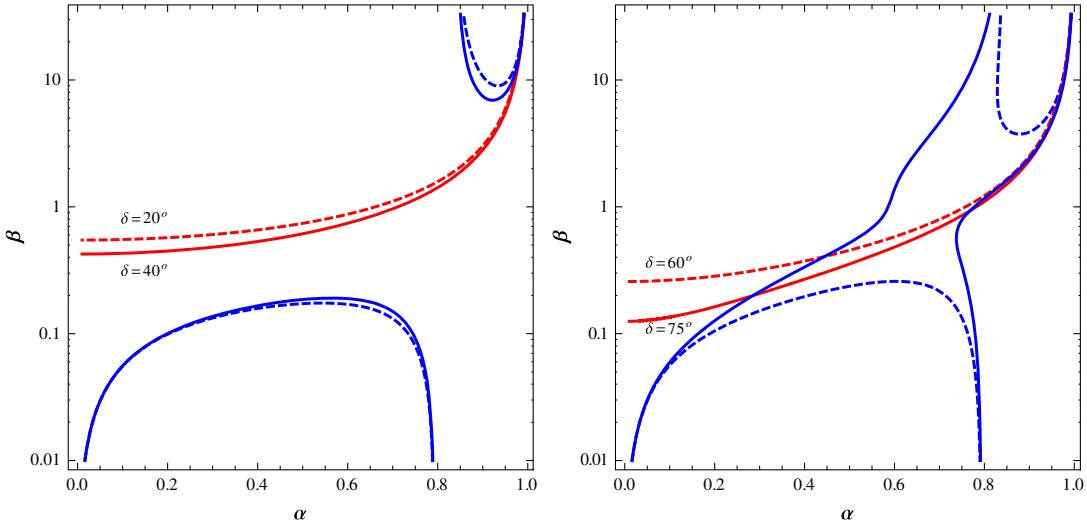

FIG. 3. Contour plots for both $\sin^2\theta_{13} = 0.0234$ (shown in red-dashed and red-continuous lines) and $r = 0.03$ (shown in blue-dashed and blue-continuous lines) in the α-β plane for various choices of δ with $\alpha < 1$. In the left panel, dashed and continuous lines represent $\delta = 20°$ and $40°$ respectively, while in the right panel, dashed and continuous lines represent contour plots for $\delta = 60°$ and $75°$ respectively.

solution as we expect is not a natural one, not only for a large value of β, but also for its very fine-tuned situation. Note that α requires to be sufficiently close (and hence finely tuned) to one in this case. This situation can be understood from the fact that β being quite large ($\gg 1$), the value of α has to be adjusted enough [see the involvement of the expression $\alpha/(1-\alpha^2)$ in Eq. (4.17)] so as to compete with the β dependent terms to get $r \sim 0.03$. Similarly variation of $\sin^2\theta_{13}$ is very sharp with respect to α (when close to 1) for large β. For example, a small change in α values ($\sim 1\%$) would induce a change in $\sin^2\theta_{13}$ by an amount of 15% near the intersection region.

However the situation changes dramatically as we proceed for higher values of δ as can be seen from Fig. 3, right panel. This figure is for two choices of $\delta = 60°$ and $75°$. We observe that with the increase of δ, the upper contour for r is extended toward the downward direction and the lower one is pushed up, thereby providing a greater chance to have an intersection with the $\sin^2\theta_{13}$ contour. We also note that the portion of $\sin^2\theta_{13}$ contour for $\alpha < 1$ prefers a region with relatively small value of $\beta(<1)$ as well. However a typical solution with both α and $\beta < 1$ appears when δ is closer to $75°$. With this δ, we could see the lower and upper contours open up to form a connected one and we can have a solution for $(\alpha, \beta) \equiv (0.29, 0.2)$. In this case, there is one more intersection between the r and $\sin^2\theta_{13}$ contours with α, $\beta < 1$ as given by (0.77, 0.93). When δ approaches $80°$ and up (until $\pi/2$) we have solutions with α, $\beta < 1$.

TABLE III. α, β values at the intersection points of the r and $\sin^2\theta_{13}$ contour plots are provided corresponding to different δ values. The sum of the light neutrino masses are also indicated in each case.

δ	α	β	$\sum m_i$(eV)
20° (160°, 200°, 340°)	0.99	28.26	0.0714
40° (140°, 220°, 320°)	0.99	20.94	0.0709
60° (120°, 240°, 300°)	0.98	11.16	0.0701
	0.94	3.70	0.0691
75° (105°, 255°, 285°)	0.77	0.93	0.0734
	0.29	0.20	0.1333
80° (100°, 260°, 280°)	0.16	0.11	0.1835
82° (98°, 262°, 278°)	0.12	0.09	0.2137
85° (95°, 265°, 275°)	0.07	0.05	0.2827

We have scanned the entire range of δ, from 0 to 2π and listed our findings in Table III. For the δ values, we denote inside the first bracket those values of δ, for which the same set of solution points (α, β) are obtained. This is due to the fact that corresponding to a r or $\sin^2\theta_{13}$ contour plot for a typical δ between 0 and 2π, the same plot is also obtained for other $|\pi - \delta|$ values. Accepting the solutions for which $\alpha, \beta < 1$ (i.e., those are not fine-tuned with large β), we find that our setup then predicts an acceptable range of CP violating Dirac phase δ to be between 72°–82°, while the first quadrant is considered. For the whole range of δ between 0 and 2π, the allowed range therefore covers 72°–82°, 98°–108°, 252°–262°, 278°–288°. Note that δ between 83° and 90° (similarly regions of δ in other quadrants also) is ruled out from the constraints on the sum of the light neutrino mass mentioned in Table III. We will discuss it shortly. Also the values of δ s like $0, \pi, 2\pi$ are disallowed in our setup as they would not produce any CP violation which is the starting point of our scenario. Again $\delta = \pi/2, 3\pi/2$ are not favored as we have not obtained any solution of α, β that satisfied both r and $\sin^2\theta_{13}$. The same is true for the case with $\alpha > 1$.

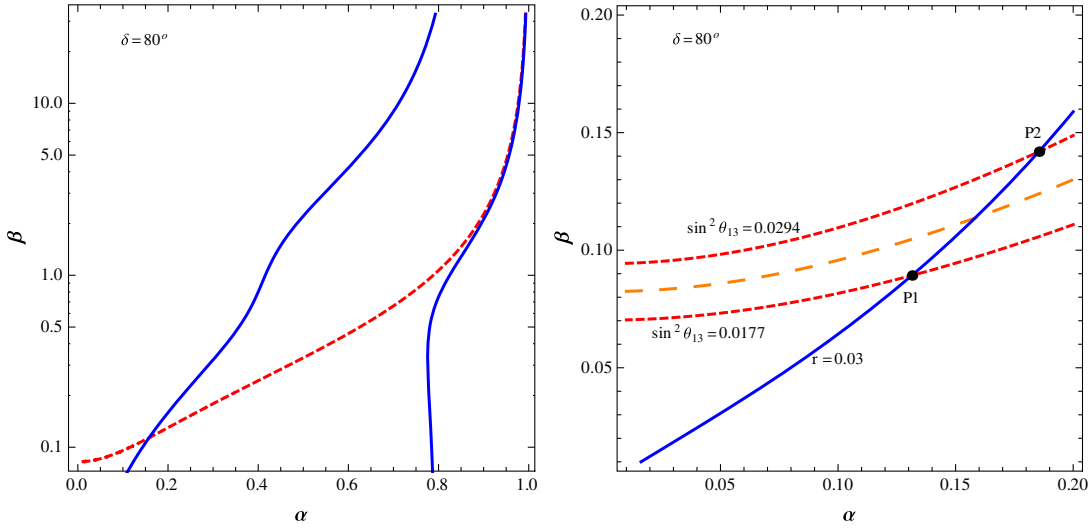

FIG. 4. The left panel contains contour plots for best-fit values of r (indicated by blue-continuous lines) and $\sin^2\theta_{13}$ (indicated by the red-dashed line) for $\delta = 80°$ in the α-β plane with $\alpha < 1$. The right panel is for the contour plot of r with its best fit value $r = 0.03$ (shown in the blue-continuous line) and 3σ range of $\sin^2\theta_{13}$ (denoted by two red-dashed lines) along with the $\sin^2\theta_{13} = 0.0234$ contour (denoted by the orange large-dashed line).

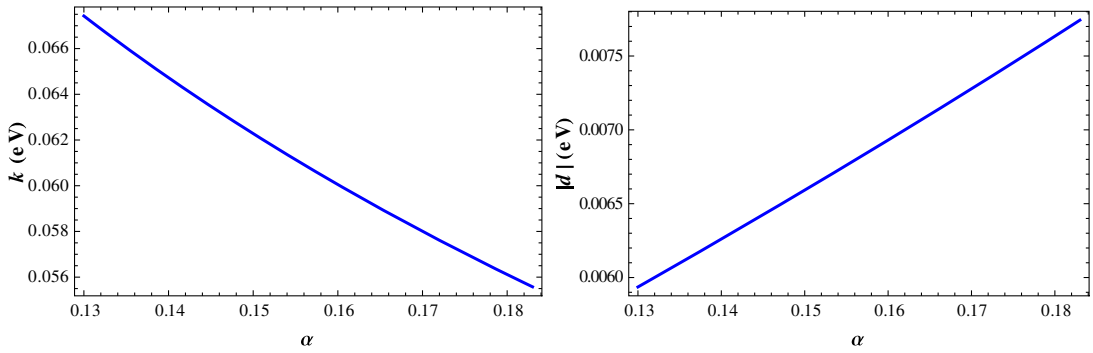

FIG. 5. k vs α (left panel) and $|d|$ vs α (right panel) for $\delta = 80°(\equiv 100°, 260°, 280°)$.

We will now proceed to discuss the prediction of the model for the light neutrino masses and other relevant quantities in terms of the parameters involved in the setup. For this, from now onward, we stick to the choice of $\delta = 80°(\equiv 100°, 260°, 280°)$ as a reference value for the Dirac *CP* violating phase. The r and $\sin^2\theta_{13}$ contours for this particular δ are shown separately in Fig. 4, left panel. In Fig. 4 (right panel) we put the $\sin^2\theta_{13}$ contours corresponding to the upper and lower values (detonated by red dotted lines) those are allowed by the 3σ range of $\sin^2\theta_{13}$. Only a section of the r contour is also incorporated which encompasses the (α, β) solution points. This plot provides a range for (α, β) once the 3σ patch of $\sin^2\theta_{13}$ is considered. It starts from a set of values $(\sim 0.13, 0.09)$ (can be called a reference point P1) up to $(\sim 0.18, 0.14)$ (another reference point P2). Note that there is always a one-to-one correspondence between the values of α and β, which falls on the line of r contour.

We have already noted that in the expression for r, parameters α, β and ϕ_d are present. Once we choose a

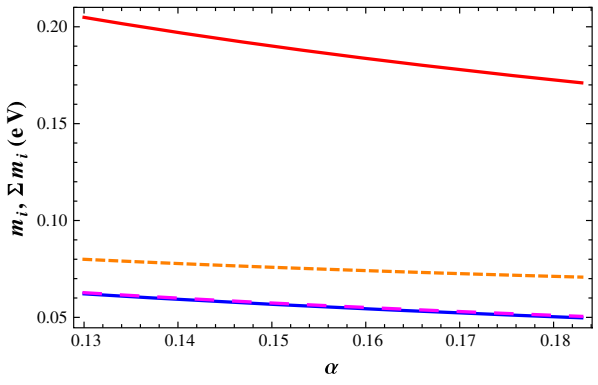

FIG. 6. Light neutrino masses m_1 (blue-continuous line), m_2 (magenta-large dashed line), m_3 (orange-dashed line) and Σm_i (red continuous line) vs α for $\delta = 80°(\equiv 100°, 260°, 280°)$.

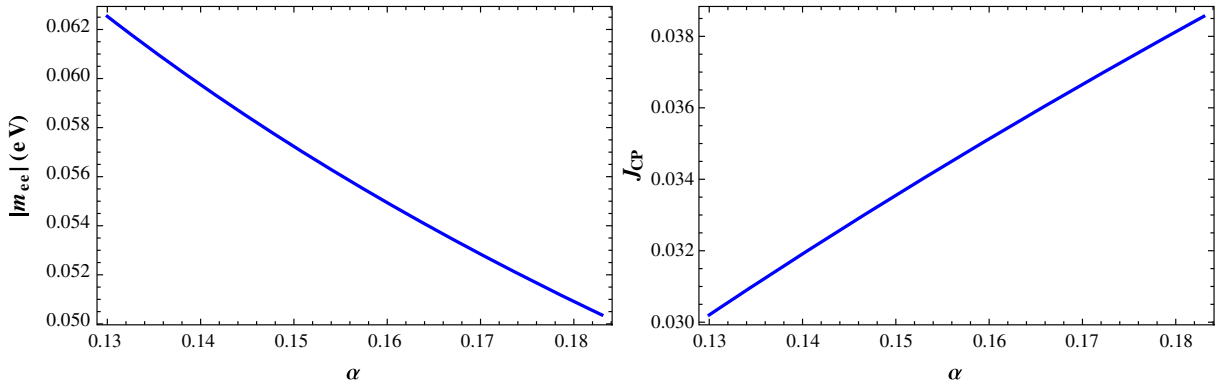

FIG. 7. Effective neutrino mass parameter (left panel) and Jarlskog invariant (right panel) vs α for $\delta = 80°(100°, 260°, 280°)$.

specific δ, automatically it boils down to find α and β from Eq. (4.17). Although r is the ratio between $\Delta m^2_{\odot}$ and $|\Delta m^2_{atm}|$, we must also satisfy the mass-squared differences $\Delta m^2_{\odot}$ as well as $|\Delta m^2_{atm}|$ independently. For that we need to determine the value of the k parameter itself apart from its involvement in the ratio $\beta = |d|/k$ as evident from Eqs. (4.10)–(4.12). For this purpose, with $\delta = 80°$ while moving from P1 to P2 along the r contour in the right panel of Fig. 4, we find the values of α and correspondingly β which produce $r = 0.03$. Now using these values of (α, β), we can evaluate the values of k for each such set which satisfies $\Delta m^2_{\odot} = 7.6 \times 10^{-5}$ eV^2. To obtain these values of k corresponding to the (α, β) set, we employ Eqs. (4.10) and (4.11). The result is reflected in the left panel of Fig. 5, where we plot the required value of k in terms of its variation with α. In producing the plot, only a narrow range of α is considered which corresponds to the 3σ variation of $\sin^2\theta_{13}$ as obtained from Fig. 4, right panel (i.e., from P1 to P2). Although we plot it against α, each value of α is therefore accompanied by a unique value of β, as we just explained. Once the variation of k in terms of α is known, we plot the variation of $|d|$ $(=\beta k)$ with α in Fig. 5, right panel. Having the correlation between α and other parameters like β, k for a specific choice of δ is known, we are able to plot the individual light neutrino masses using Eqs. (4.10)–(4.12). This is done in Fig. 6. The light neutrino masses satisfies normal mass hierarchy. We also incorporate the sum of light neutrino masses (Σm_i) to check its consistency with the cosmological limit set by Planck, $\Sigma m_i < 0.23$ eV [67]. In this particular case with $\delta = 80°$ (also for $\delta = 100°, 260°, 280°$), this limit is satisfied for the allowed range of α, it turns out that $\delta = 83°$ and $97°$ (and similarly for 263°–277°) do not satisfy it as indicated in Table III. One can check that indeed the light neutrino masses are mostly dominated by the type-I seesaw contribution. This can be seen from Eqs. (4.10)–(4.12) by setting $\beta = 0$. As an example, with $\delta = 80°$ ($\alpha < 1$ case), m_3 is found to be 0.074 eV and the type-I contribution toward this mass is almost 0.07 eV. A similar conclusion holds for other ranges of δ values as well.

Now by using Eqs. (4.15)–(4.16), we estimate the Majorana phases[4] α_{21} and α_{31} for $\delta = 80°$, which appears in the effective neutrino mass parameter $|m_{ee}|$. $|m_{ee}|$ appears in evaluating the neutrinoless double beta decay and is given by [65],

$$|m_{ee}| = |m_1^2 c_{12}^2 c_{13}^2 + m_2^2 s_{12}^2 c_{13}^2 e^{i\alpha_{21}} + m_3^2 s_{13}^2 e^{i(\alpha_{31}-2\delta)}|. \tag{4.18}$$

In Fig. 7, we plot the prediction of $|m_{ee}|$ against α within its narrow range satisfying the 3σ range of $\sin^2\theta_{13}$ with $\delta = 80°$. Here we obtain $0.050 \leq |m_{ee}| \leq 0.062$. This could be probed in future generation experiments providing a testable platform of the model itself.

It is known that the presence of the nonzero Dirac CP phase can trigger CP violation in neutrino oscillation at low energy. In standard parametrization, the magnitude of this CP violation can be estimated [65] through

$$\begin{aligned} J_{CP} &= \mathrm{Im}[U_{\mu 3} U_{e3}^* U_{e2} U_{\mu 2}^*] \\ &= \frac{1}{8}\cos\theta_{13} \sin 2\theta_{12} \sin 2\theta_{23} \sin 2\theta_{13} \sin\delta. \end{aligned} \tag{4.19}$$

As in our model, the unique source of δ is the CP violating phase α_S in S, it is interesting to see the prediction of our model towards J_{CP}. Using the expression of J_{CP} in Eq. (4.19) along with Eqs. (4.5) and (4.6) we estimate J_{CP} in our model as shown in Fig. 7 (right panel) with $\delta = 80°$. Here also we include only that range of α which provides solutions corresponding to the 3σ allowed range of $\sin^2\theta_{13}$. However we scanned the entire range of α where the solutions exist for all allowed values of δ and find that J_{CP} in our model is predicted to be $0.03 < |J_{CP}| < 0.04$. This can be measured in future neutrino experiments.

[4]The source of these phases is the phase ϕ_d only.

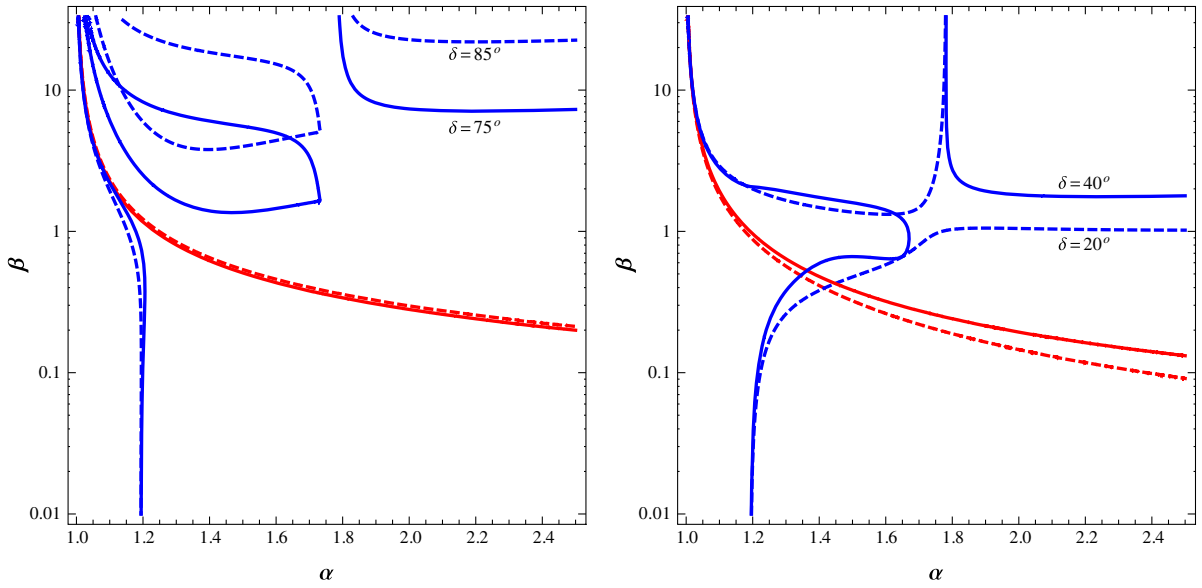

FIG. 8. Contour plots for both $\sin^2\theta_{13} = 0.0234$ (shown in red-dashed and red-continuous lines) and $r = 0.03$ (shown in blue-dashed and blue-continuous lines) in the α-β plane for various choices of δ with $\alpha > 1$. In the left panel, dashed and continuous lines represent $\delta = 85°$ and $75°$ respectively, while in the right panel, dashed and continuous lines represent contour plots for $\delta = 20°$ and $40°$ respectively.

B. Results for case B

Similar to case A, we consider here the expression of r for $\alpha > 1$ from Eq. (4.17) to draw the contour plot for $r = 0.03$ in the α-β plane as shown in Fig. 8 while δ is fixed at different values. In the same plot we include the $\sin^2\theta_{13} = 0.0234$ contour as well to find the set of parameters (α, β) corresponding to a fixed δ which satisfies the best fit values of $\sin^2\theta_{13}$ and r. Once we restrict β to be below one, we find the solutions to exist for $\delta = 0°$–$63°$, ($117°$–$180°$, $180°$–$243°$, $297°$–$360°$) shown in Table IV. For δ's beyond $63°$ (when considered within $\pi/2$), the solutions exhibit $\beta \gg 1$ implying a fine-tuned situation similar to case A. Note that α therefore falls in a narrow range $\simeq$1.2–1.4 in order to satisfy both $\sin^2\theta_{13} = 0.0234$ and $r = 0.03$ considering all δ

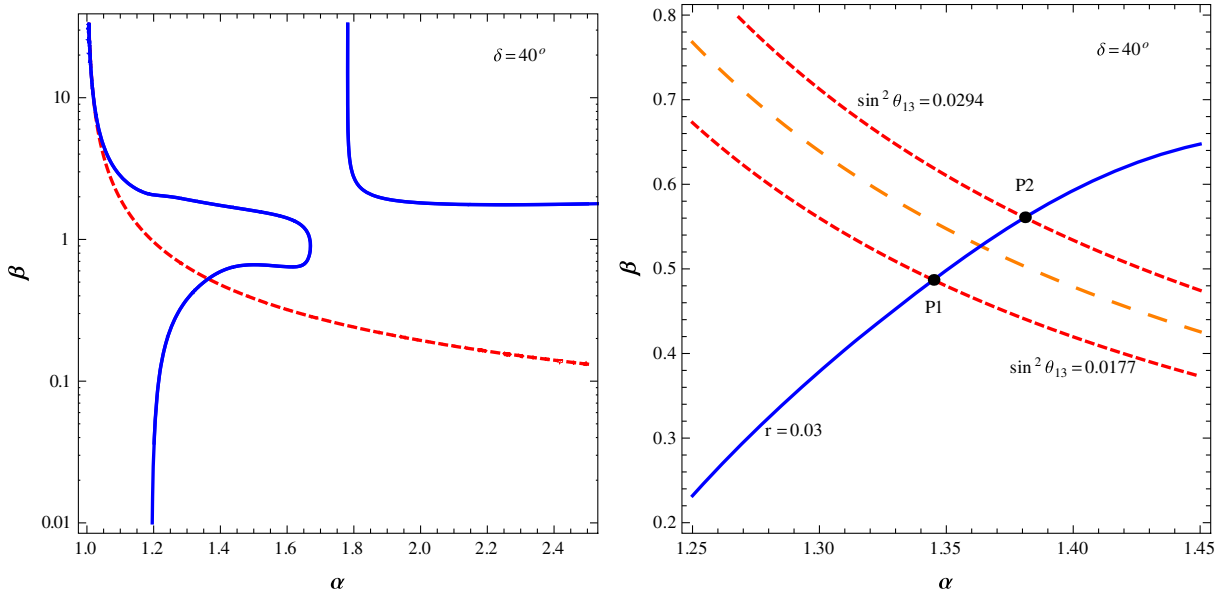

FIG. 9. The left panel contains contour plots for best-fit values of r (indicated by blue-continuous lines) and $\sin^2\theta_{13}$ (indicated by the red-dashed line) for $\delta = 40°$ in the α-β plane with $\alpha > 1$. The right panel is for the contour plot of r with its best fit value $r = 0.03$ (shown in the blue-continuous line) and 3σ range of $\sin^2\theta_{13}$ (denoted by two red-dashed lines) along with the $\sin^2\theta_{13} = 0.0234$ contour (denoted by the orange large-dashed line).

TABLE IV. Solutions for $\alpha(>1)$ and β for various δ.

δ	α	β	$\sum m_i$(eV)
10° (170°, 190°, 350°)	1.43	0.36	0.0791
30° (150°, 210°, 330°)	1.39	0.45	0.0798
40° (140°, 220°, 320°)	1.36	0.53	0.0799
50° (130°, 230°, 310°)	1.32	0.64	0.0794
60° (120°, 240°, 300°)	1.26	0.83	0.0776
70° (110°, 250°, 290°)	1.17	1.13	0.0739
73° (107°, 253°, 287°)	1.07	3.02	0.0696

values. In Fig. 9 (left panel), we find the intersection is at (1.36, 0.53) for $\delta = 40°(\equiv 140°, 220°, 320°)$. Considering this δ as a reference for discussion, we further include the 3σ range of $\sin^2\theta_{13}$ in Fig. 9 (right panel). We find α to be varied between 1.35 and 1.39 while $\sin^2\theta_{13}$ changes from the lower to the higher value, within the 3σ limit. Within this range, we predict individual light neutrino masses and their sum. Here also we find normal hierarchy for them as seen from Fig. 10. With $\alpha > 1$, we find that the type-I contribution toward physical neutrino masses dominates similar to the case with $\alpha < 1$. For example, with $m_3 = 0.057$ eV, the type-I part is ~0.062 eV [obtained by setting $\beta = 0$ in Eq. (4.12)] and hence the triplet contribution is almost 1 order of magnitude less compared to type-I contribution. For different δ-values, the Σm_i (corresponding to the best fit value of $\sin^2\theta_{13}$) are provided in Table IV. For showing the prediction of our model in terms of other quantities like $|m_{ee}|$ and J_{CP}, the left and right panels of Fig. 11 are included. Considering all the δ values for which $\beta \leq 1$, we find $|J_{CP}|$ to be within $|J_{CP}| < 0.035$.

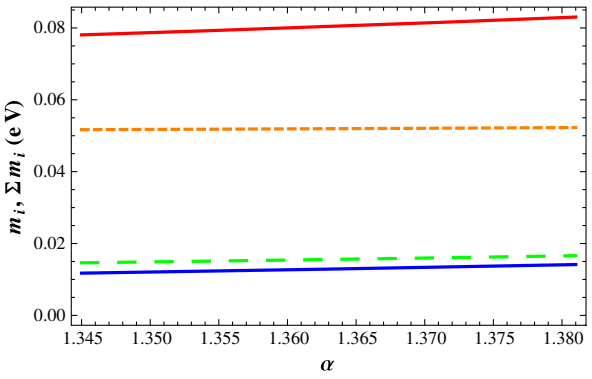

FIG. 10. Light neutrino masses m_1 (blue-continuous line), m_2 (green-large dashed line), m_3 (orange-dashed line) and Σm_i (red continuous line) vs α (>1 case) for $\delta = 40°(\equiv 140°, 220°, 320°)$.

V. LEPTOGENESIS

In a general type-II seesaw framework, leptogenesis can be successfully implemented through the decay of RH neutrinos [72] or from the decay of the triplet(s) involved [73–77] or in a mixed scenario where both RH neutrino and the triplet(s) contribute [78–83]. In the present setup, all the couplings involved in the pure type-I contribution are real and hence the neutrino Yukawa matrices and the RH neutrino mass matrices do not include any CP violating phase. Therefore CP asymmetry originated from the sole contribution of RH neutrinos is absent in our framework. As we have mentioned earlier, the source of CP violation is only present in the triplet contribution and that is through the vev of the S field. However as it is known [76,84], a single $SU(2)_L$ triplet does not produce CP-asymmetry. Therefore there are two remaining possibilities to generate successful lepton asymmetry [80,85] in the present context; (I) from the decay of the triplet where the one-loop diagram involves the virtual RH neutrinos and (II) from the decay of the RH neutrinos where the one-loop contribution involves the virtual triplet running in the loop. Provided the mass of the triplet is light compared to all the RH neutrinos (i.e., $M_\Delta < M_{Ri}$), we consider option (I). Once the triplet is heavier than the RH neutrinos, we explore option (II).

First we consider option (I), i.e., when $M_\Delta < M_{Ri}$. At tree level the scalar triplet can decay either into leptons or into two Higgs doublets, followed from the Lagrangian in Eqs. (3.9) and (3.12). For $\Delta \to LL$, the one-loop diagram

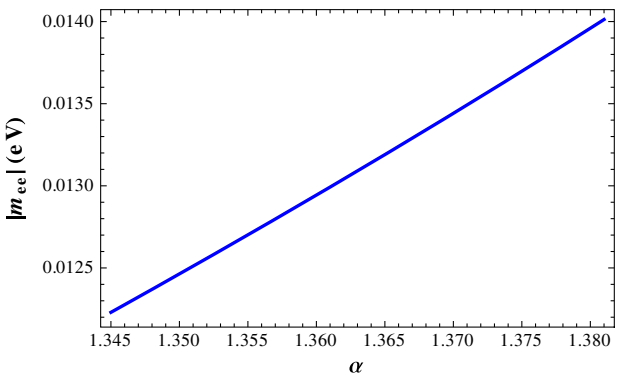

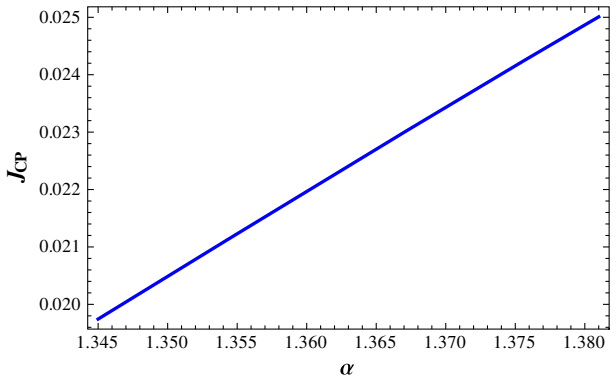

FIG. 11. Effective neutrino mass parameter (left panel) and Jarlskog invariant (right panel) vs α for $\delta = 40°(\equiv 140°, 220°, 320°)$ when $\alpha > 1$.

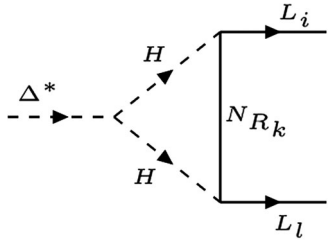

FIG. 12. One-loop diagram which contributes to the generation of ϵ_Δ.

involves the virtual RH neutrinos running in the loop as shown in Fig. 12. Interference of the tree level and the one-loop results in the asymmetry parameter [73,80,86]

$$\epsilon_\Delta = 2\frac{\Gamma(\Delta^* \to L+L) - \Gamma(\Delta \to \bar{L}+\bar{L})}{\Gamma(\Delta^* \to L+L) + \Gamma(\Delta \to \bar{L}+\bar{L})}, \quad (5.1)$$

$$= \frac{1}{8\pi}\sum_k M_{Rk}\frac{\sum_{il}\mathrm{Im}[(\hat{Y}_D^*)_{ki}(\hat{Y}_D^*)_{kl}(Y_\Delta)_{il}\eta^*]}{\sum_{ij}|(Y_\Delta)_{ij}|^2 M_\Delta^2 + |\eta|^2} \times \log(1 + M_\Delta^2/M_{Rk}^2). \quad (5.2)$$

Here i, j denote the flavor indices, $\hat{Y}_D = U_R^T Y_D$ in the basis where the RH neutrino mass matrix is diagonal. Y_Δ, Y_D and expression of η can be obtained from Eqs. (3.5), (3.10) and (3.13). Masses of RH neutrinos can be expressed as

$$M_{R_1} = \frac{v^2 y^2}{k}(1+\alpha), \quad (5.3)$$

$$M_{R2} = \frac{v^2 y^2}{k}, \quad (5.4)$$

$$M_{R_3} = \left|\frac{v^2 y^2}{k}(1-\alpha)\right|. \quad (5.5)$$

Therefore, in the limit when the scalar triplet is much lighter than the RH neutrinos, the asymmetry parameter in our model is estimated to be [80]

$$\epsilon_\Delta = -\frac{M_\Delta^2}{8\pi v^2}\frac{\alpha^2}{(1-\alpha^2)} \times \frac{k\mu\tilde{\omega}^3 v_S (x_1 - x_1')\sin\alpha_S}{[3\tilde{\omega}^2\frac{v_S^2}{\Lambda^2}(x_1^2 + x_1'^2 + 2x_1x_1'\cos 2\alpha_S)M_\Delta^2 + (\mu\tilde{\omega}^2\Lambda)^2]}. \quad (5.6)$$

Here we denote $\tilde{\omega} = v_f/\Lambda$, where v_f is considered to be the common vev of all flavons except S-field's vev $\langle S\rangle = v_S e^{i\alpha_S}$. The associated phase α_S is the only source of *CP*-violation here. The total decay width of the triplet Δ (for $\Delta \to$ two leptons and $\Delta \to$ two scalar doublets) is given by

$$\Gamma_T = \Gamma_{\Delta^* \to LL} + \Gamma_{\Delta^* \to HH} \quad (5.7)$$

$$= \frac{M_\Delta}{8\pi}\left[\sum_{ij}|(Y_\Delta)_{ij}|^2 + \frac{|\eta|^2}{M_\Delta^2}\right]. \quad (5.8)$$

Note that there are few parameters in Eq. (5.6), e.g., α, k which already contributed in determining the mass and mixing for light neutrinos. Also ϕ_d is related with α_S by Eq. (4.9). In the previous section, we have found solutions for (α, β) that satisfy the best fit values of $\sin^2\theta_{13}$ and r for a specific choice of δ (the reference values $\delta = 80°$ for $\alpha < 1$ and $\delta = 40°$ for $\alpha > 1$). Then we can find the values of k and $|d|$ corresponding to that specific δ value. These sets of α, $|d|$, k produce the correct order of neutrino mass and mixing as we have already seen. Here to discuss the *CP*-asymmetry parameter ϵ_Δ, we therefore choose $\delta = 80°(100°, 260°, 280°)$ for $\alpha < 1$ and $\delta = 40°(140°, 220°, 320°)$ for $\alpha > 1$.

We further define $v_S/\Lambda = f\tilde{\omega}$ where f serves as a relative measure of the vevs. With this, the expression of ϵ_Δ takes the form

$$\epsilon_\Delta = -\frac{\alpha^2}{8\pi v^2(1-\alpha^2)} \times \frac{kf(x_1 - x_1')\sin\alpha_S(\mu\Lambda/M_\Delta^2)}{[(3f^2/M_\Delta^2)(x_1^2 + x_1'^2 + 2x_1x_1'\cos 2\alpha_S) + (\mu\Lambda/M_\Delta^2)^2]}, \quad (5.9)$$

which is $\tilde{\omega}$ independent. The expression for $|d|$ as obtained from Eq. (3.15) can be written as

$$|d| = 2fv^2\tilde{\omega}^4\frac{\mu\Lambda}{M_\Delta^2}(x_1 + x_1')\cos\alpha_S \sec\phi_d. \quad (5.10)$$

Using Eq. (5.9), we obtain the contour plot for $\epsilon_\Delta = 10^{-6}$, 10^{-7}, 10^{-8} with $\mu = 1$, $f = 0.1$, $x_1 = 0.5$ and $x_1' = 1$ which are shown in Fig. 13, left panel. The electroweak vev is also inserted in the expression. In obtaining the plots we varied Λ above the masses of RH neutrinos [Eqs. (5.3)–(5.5)]. The variation of M_Δ is also restricted from above by the condition that we work in regime (I) where $M_\Delta < M_{R_{i=1,2,3}}$. Figure 13 is produced for a specific choice of $\delta = 80°(100°, 260°, 280°)$ which corresponds to the solution $(\alpha = 0.16, \beta = 0.11)$. The values of $|d|$ and k corresponding to this set of (α, β) are found to be 0.0068 and 0.06 eV respectively. Note that $M_\Delta < M_{Ri}$ restricts the choice of y involved in Eqs. (5.3)–(5.5). We have chosen $y = 1$ for the left panel of Fig. 13. In order to keep $M_\Delta < M_{Ri} < \Lambda$, we find $M_\Delta \simeq 10^{13-14}$ GeV would be the right choice for enough lepton asymmetry can be generated. As the values of α, k are fixed for generating the plots of Fig. 13, following Eqs. (5.3)–(5.5) the corresponding RH neutrino masses are found to be $M_{R_1} = 5.8 \times 10^{14}$ GeV, $M_{R_2} = 5.01 \times 10^{14}$ GeV and $M_{R_3} = 4.22 \times 10^{14}$ GeV (with $y = 1$).

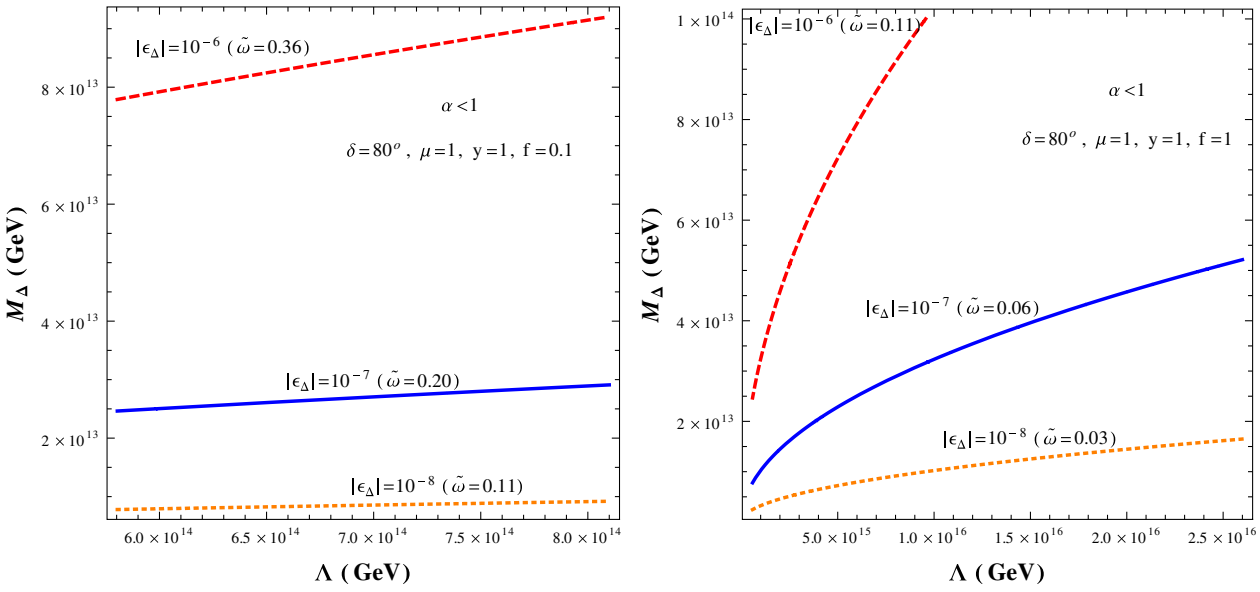

FIG. 13. Contours corresponding to different values of $|\epsilon_\Delta|$ in the $M_\Delta - \Lambda$ plane with $\alpha < 1$. The choice of other parameters are provided inside the figures.

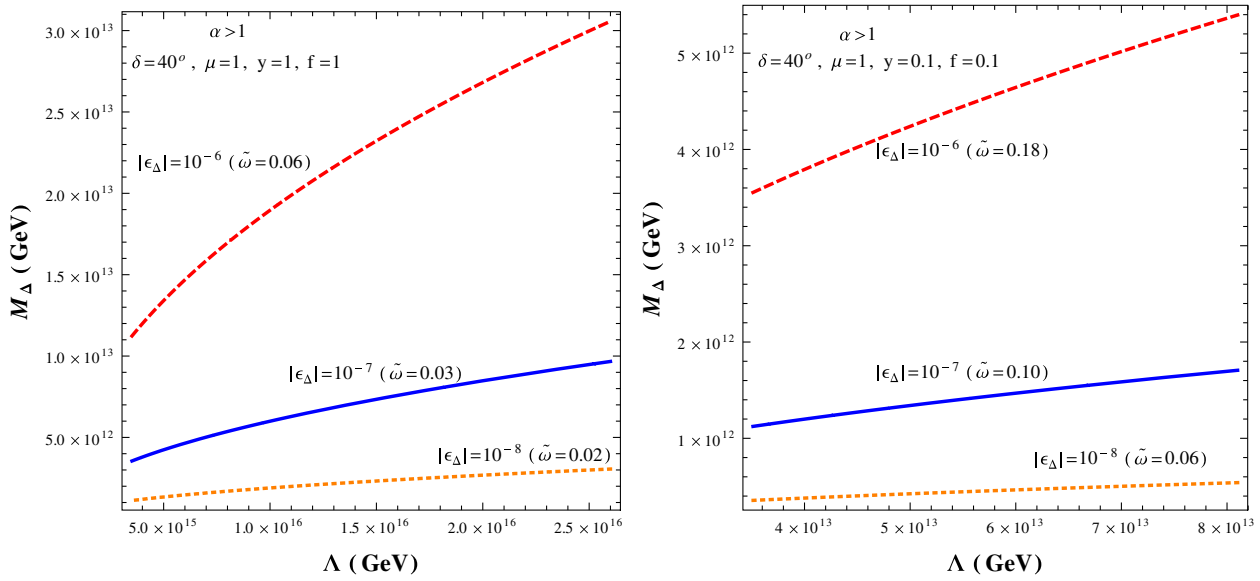

FIG. 14. Contours corresponding to different values of $|\epsilon_\Delta|$ in the $M_\Delta - \Lambda$ plane with $\alpha > 1$. The choice of other parameters are provided inside the figures.

Note that value of $\tilde{\omega}$ can be concluded from the expression of $|d|$ in Eq. (5.10), for a choice of Λ/M_Δ^2 which produces a ϵ_Δ contour. This is because corresponding to a specific choice of δ value, $|d|$ is uniquely determined for the solution point (α, β). Hence with fixed values of x_1, x_1', f, μ (with the same values to have the ϵ_Δ contour), $\tilde{\omega}$ can be evaluated from $|d|$ for a chosen Λ/M_Δ^2. It turns out that $\tilde{\omega}$ has a unique value for a specific ϵ_Δ for both panels of Fig. 13. For example, with $\epsilon_\Delta = 10^{-7}$, we need $\tilde{\omega} = 0.2$, while to have $\epsilon_\Delta = 10^{-6}$, $\tilde{\omega}$ is required to be 0.36. These $\tilde{\omega}$ values are provided in the first bracket in each figure beside the ϵ_Δ value. The reason is the following. For the specified range of Λ (i.e., $M_\Delta < M_{Ri} < \Lambda$), it follows that[5] the first bracketed term in the denominator of Eq. (5.9) is almost negligible compared to the second term (with the

[5]In principle, the operator $LHLH$ contributes in the present framework at a higher order, with the $\frac{c_1}{\Lambda^2} LHLH\xi$ (ϕ_S) term. However its contribution is suppressed compared to the type-I contribution by $\sim\tilde{\omega}^2 \ll 1$, with $c_1 \sim \mathcal{O}(1)$. It turns out that with the parameters specified in our discussion, it is also smaller [with $c_1 \sim \mathcal{O}(1)$] than the triplet contribution.

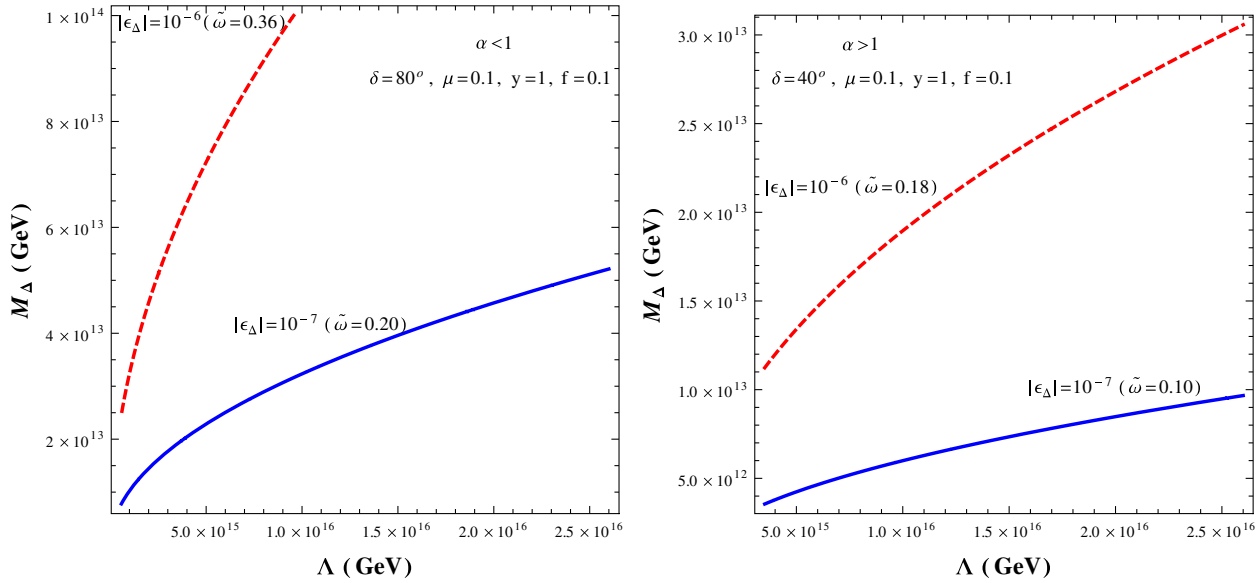

FIG. 15. Contours corresponding to different values of $|\epsilon_\Delta|$ in the $M_\Delta-\Lambda$ plane for $\alpha<1$ (left panel) and $\alpha>1$ (right panel) with relatively small $\mu(=0.1)$. The choice of other parameters are provided inside the figures.

choice of x_1, x_1', f, μ as mentioned before) and hence effectively

$$\epsilon_\Delta \simeq -\frac{\alpha^2}{8\pi v^2(1-\alpha^2)} kf(x_1-x_1')\sin\alpha_S \frac{M_\Delta^2}{\mu\Lambda}. \qquad (5.11)$$

Therefore for a typical choice of ϵ_Δ, Λ/M_Δ^2 is almost fixed and the $|d|$ expression in Eq. (5.11) tells that $\tilde{\omega}$ also is almost fixed. In the right panel of Fig. 13, we take $y=1$, $f=1$ and draw the contours for ϵ_Δ while x_1, x_1', μ are fixed at their previous values considered for generating plots in the left panel. In this case, M_Δ turns out to be $10^{13\text{–}14}$ GeV.

Similarly, contours for ϵ_Δ are drawn in Fig. 14 for the $\alpha>1$ case. Correspondingly, we have used solutions of ($\alpha=1.36$, $\beta=0.53$) and the values of $k=0.02$ eV and $|d|=0.01$ eV are taken for $\delta=40°$ (also for 140°, 220°, 320°). For the left panel of Fig. 14, $\mu=1$, $y=1$ and $f=1$ are considered and we get a somewhat lighter scalar with mass, $M_\Delta\sim 10^{13}$ GeV. In this case the RH neutrinos are with masses $M_{R_1}=3.5\times10^{15}$GeV, $M_{R_2}=1.48\times10^{15}$ GeV and $M_{R_3}=5.4\times10^{14}$ GeV and hence satisfying $M_\Delta<M_{Ri}$. For the right panel of Fig. 14, y is considered as 0.1 and hence the RH neutrino masses are smaller compared to the left panel. However, they are still heavier (here the lightest RH neutrino mass, $M_{R_3}=5.4\times10^{12}$ GeV) than the scalar triplet, $M_\Delta\sim10^{12}$ GeV. In Fig. 15 similar contour plots for ϵ_Δ are exercised with μ at somewhat lower values, fixed at $\mu=0.1$ along with $f=0.1$ for both $\alpha<1$ (left panel) and $\alpha>1$ (right panel). Corresponding to Fig. 15, the masses of the RH neutrinos are $M_{R_1}=5.8\times10^{14}$ GeV, $M_{R_2}=5.01\times10^{14}$ GeV, $M_{R_3}=4.22\times10^{14}$GeV for $\alpha<1$ (left panel) and $M_{R_1}=3.5\times10^{15}$GeV, $M_{R_2}=1.48\times10^{15}$GeV, $M_{R_3}=5.4\times10^{14}$ GeV for $\alpha>1$ (right panel). So the choice of y satisfies $M_\Delta<M_{Ri}$ for the range of M_Δ considered in Fig. 15.

So overall we have found that enough ϵ_Δ can be created so as to achieve the required lepton asymmetry through $\frac{n_L}{n_\gamma}=\epsilon_\Delta\frac{n_\Delta}{n_\gamma}D$ with $n_\Delta=n_{\Delta_0}+n_{\Delta_+}+n_{\Delta_{++}}$ is the total number density of the triplet and D is the efficiency factor. After converting it into baryon asymmetry by the sphaleron process, n_B/n_γ is given by $\frac{n_B}{n_\gamma}\simeq-0.03\epsilon_\Delta D$. D depends on the satisfaction of the out-of-equilibrium condition ($\Gamma_\Delta\lesssim H|_{T=M_\Delta}$). Being $SU(2)_L$ triplet, it also contains the gauge interactions. Hence the scattering like $\Delta\Delta\to$ SM particles can be crucial [87,88]. In [75,76,80,89,90], it has been argued that even if the triplet mass (M_Δ) is much below 10^{14} GeV, the triplet leptogenesis mechanism considered here is not affected much by the gauge mediated scatterings. The exact estimate of D requires to solve the Boltzmann equations in detail which is beyond the scope of the present paper.[6] However analysis toward evaluating D in this sort of framework (where a single triplet is present and RH neutrinos are in the loop for generating ϵ_Δ) exits in [76]. Following [76], we note that with the effective type-II mass $\tilde{m}_\Delta(\equiv\sqrt{\mathrm{Tr}(m_\nu^{II\dagger}m_\nu^{II})})\sim(0.01\text{–}0.02)$ eV, the efficiency D is of the order of 10^{-3}. In estimating[7] $\tilde{m}_\Delta$, we have considered all the parameters in a range (mentioned

[6]A detailed study on flavor effects in scalar triplet leptogenesis can be found in [91].

[7]It is possible to recast Eq. (5.2) as $\epsilon_\Delta=-\frac{1}{8\pi}\frac{M_\Delta}{v^2}\sqrt{B_L B_H}\frac{\mathrm{Tr}(m_\nu^{l\dagger}m_\nu^{ll})}{\tilde{m}_\Delta}$ with the consideration $M_\Delta<M_{Rk}$. Here B_L and B_H are corresponding branching ratio's of decay of the triplet into two leptons and two scalar doublets.

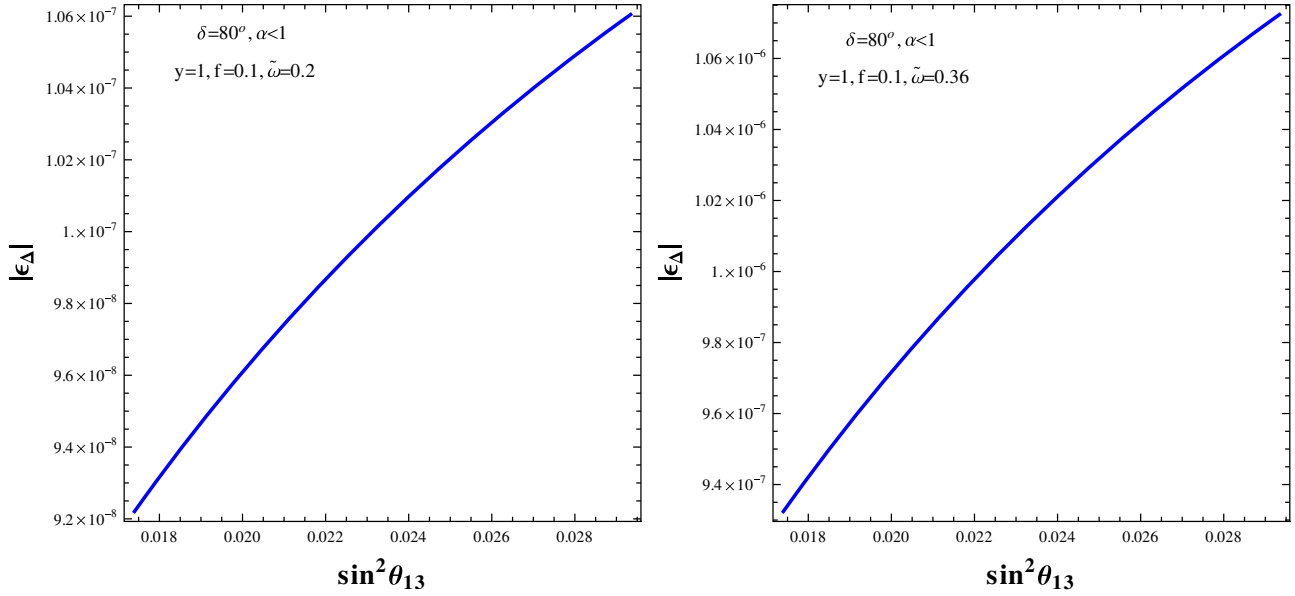

FIG. 16. Variation of $|\epsilon_\Delta|$ with $\sin^2\theta_{13}$ for $\alpha < 1$. The left panel is with $\tilde{\omega} = 0.2$ while the right panel is with $\tilde{\omega} = 0.36$.

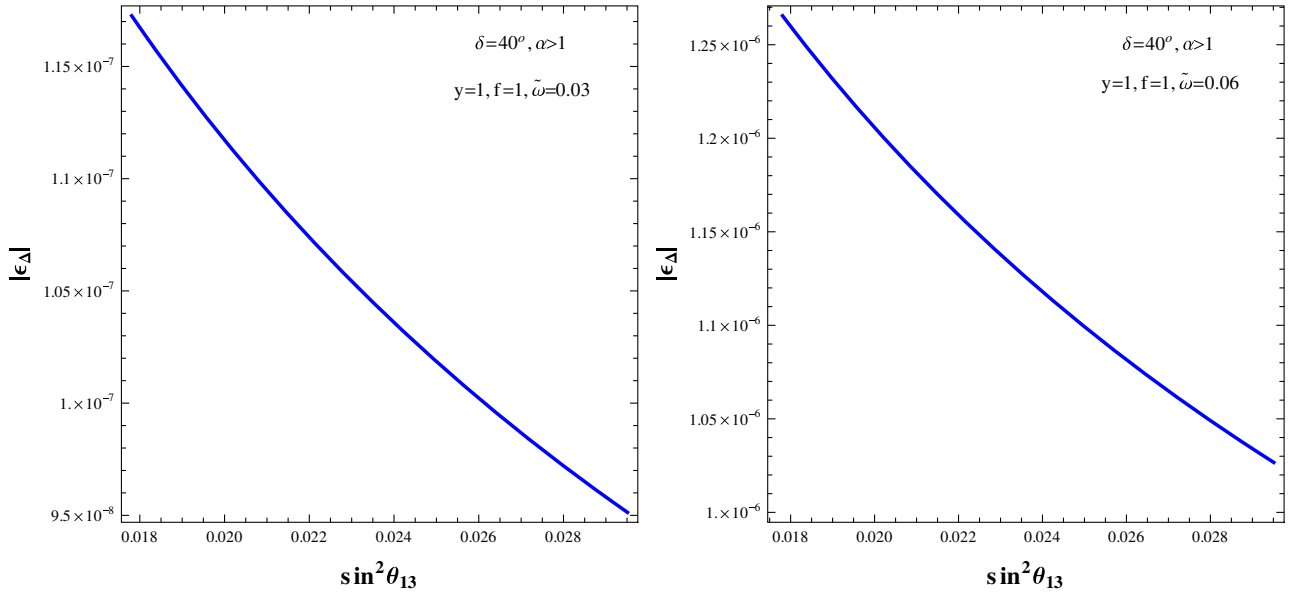

FIG. 17. Variation of $|\epsilon_\Delta|$ with $\sin^2\theta_{13}$ for $\alpha > 1$. The left panel is with $\tilde{\omega} = 0.03$ while the right panel is with $\tilde{\omega} = 0.06$.

within Figs. 13 and 14) so as to produce ϵ_Δ of order 10^{-6} as shown in Figs. 13 and 14.

Now, using the approximated expression as given by Eq. (5.11) we can obtain variation of $|\epsilon_\Delta|$ against $\sin^2\theta_{13}$ as given in Fig. 16 for $\alpha < 1$ and in Fig. 17 with $\alpha > 1$. In doing so we have substituted $\mu\Lambda/M_\Delta^2$ from Eq. (5.10) in Eq. (5.11). Then as discussed in the previous section, using solutions of α, β for 3σ range of $\sin^2\theta_{13}$ with fixed δ value, we have obtained Figs. 16 and 17 for $\alpha < 1$ and $\alpha > 1$ respectively. Here Fig. 16 for $\delta = 80°(100°, 260°, 280°)$ and Fig. 17 with $\delta = 40°(140°, 220°, 320°)$.

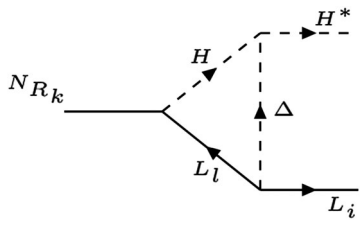

FIG. 18. One-loop diagram for decay of RH neutrinos.

It is interesting to note that within our present framework, neutrino oscillation data imposes an upper bound on the lepton asymmetry as seen from Fig. 16 (Fig. 17) corresponding to the upper (lower) value of $\sin^2\theta_{13}$ within the 3σ range for $\alpha < 1$ ($\alpha > 1$). Although a value of $|\epsilon_\Delta| \sim 10^{-7}$ as found in Fig. 16 seems to be quite restrictive for

leptogenesis in the present context, a somewhat generous value of $|\epsilon_\Delta| \sim 10^{-6}$ can be obtained in our case by a change of value of $\tilde{\omega}$ from 0.2 to $\tilde{\omega} = 0.36$ as seen by comparing the left and the right panel of Fig. 16. Similar conclusions hold for the $\alpha > 1$ case also as seen from Fig. 17.

We now discuss option II, when RH neutrinos are lighter than M_Δ. The one loop diagram involves here the virtual triplet (Δ) running in the loop as shown in Fig. 18. The contribution toward the CP-asymmetry parameter generated from the decay of the lightest neutrino is given by

$$\epsilon_{N_1} = \frac{3}{16\pi v^2} M_{R_1} \frac{\sum_{il} \mathrm{Im}[(\hat{Y}_D)_{1i}(\hat{Y}_D)_{1l}(m_\nu^{II*})_{il}]}{\sum_i |(\hat{Y}_D)_{1i}|^2}, \tag{5.12}$$

$$= \frac{3M_{R_1}}{2} \frac{1}{16\pi v^2} |d| \sin\phi_d, \tag{5.13}$$

$$\epsilon_{N_2} = -3M_{R_2} \frac{1}{16\pi v^2} |d| \sin\phi_d \quad \text{and}$$

$$\epsilon_{N_3} = \mp \frac{3M_{R_3}}{2} \frac{1}{16\pi v^2} |d| \sin\phi_d, \tag{5.14}$$

where we have used m_ν^{II} from Eq. (3.14). In the above, "+" and "−" sign stands for $\alpha > 1$ and $\alpha < 1$ cases respectively in the computation of ϵ_{N_3}. The above expressions of ϵ_{N_i} are valid when the scalar triplet is much heavier than the singlet RH neutrinos. Note that in the present scenario, the RH neutrino masses are not entirely hierarchical, rather they are closely placed. Therefore the total baryon asymmetry from the decay of the three RH neutrinos is to be estimated as $|\frac{n_B}{s}| = 1.48 \times 10^{-3} \sum_i \epsilon_{N_i} D_{N_i}$, where D_{N_i} is the respective efficiency factor. It turns out that with the same D_{N_i} for $i = 1, 2, 3$, $\sum_i \epsilon_{N_i} = 0$ as a result [using M_{R_i} from Eq. (5.5)] of the specific flavor structure considered. Therefore it is expected that the lepton asymmetry would be suppressed in this case. Also in this case $M_{R_i} < M_\Delta$, which can be obtained by considering the smaller value of the Yukawa coupling y (as to generate the required $|d|$, specific values of α, β, k are already chosen). This could reduce the individual ϵ_{N_i}. We conclude this contribution (ϵ_N) as a subdominant to ϵ_Δ.

VI. CONCLUSION

We have considered a flavor symmetric framework for generating light neutrino masses and mixing through the type-II seesaw mechanism. In realizing it, we have introduced three SM singlet RH neutrinos, one $SU(2)_L$ triplet and few flavon fields. The RH neutrinos contribute to the type-I term, which guided by the $A_4 \times Z_4 \times Z_3$ symmetry of the model produces a TBM mixing pattern. Then we have shown that the typical flavor structure resulted from the model can generate nonzero θ_{13}. In this framework, all the couplings are considered to be real. The CP symmetry is violated spontaneously by the complex vev of a single SM singlet field, while other flavons have real vevs. Interestingly this particular field is involved only in the pure type-II term. Hence the triplet contribution not only generates the θ_{13}, it is also responsible for providing Dirac CP violating phase δ. Therefore the model has the potential to predict δ in terms of the parameters involved in neutrino masses and mixing. We have therefore studied the parameter space of the setup considering that the triplet contribution is subdominant or at most comparable to the type-I term. The model indicates the values of δ to be in the range 72°–82°, 98°–108°, 252°–262°, 278°–288° for $\alpha < 1$ and $\delta = 0°$–$63°$, 117°–180°, 180°–243°, 297°–360° for $\alpha > 1$. However $\delta = 0$ (and hence π, 2π) is disfavored in our scenario as in that case no CP violation would be present. Also $\delta = \pi/2$, $3\pi/2$ are excluded here. These ranges can be tested in future neutrino experiments. We provide an estimate for the J_{CP}. The sums of the neutrino masses are also evaluated. It turns out that the scenario works with normal hierarchical masses of light neutrinos. We have also studied leptogenesis in this model. As the type-I contribution to the light neutrino mass does not involve any CP violating phase, RH neutrinos decay cannot contribute to the lepton asymmetry in the conventional way. We have found the triplet decay with the virtual RH neutrino in the loop can produce enough lepton asymmetry.

[1] P. Minkowski, $\mu \to e\gamma$ at a rate of one out of 10^9 muon decays?, Phys. Lett. B **67**, 421 (1977).

[2] M. Gell-Mann, P. Ramond, and R. Slansky, Complex spinors and unified theories, Conf. Proc. C **790927**, 315 (1979).

[3] R. N. Mohapatra and G. Senjanovic, Neutrino Mass and Spontaneous Parity Violation, Phys. Rev. Lett. **44**, 912 (1980).

[4] T. Yanagida, Horizontal symmetry and masses of neutrinos, Prog. Theor. Phys. **64**, 1103 (1980).

[5] P. F. Harrison, D. H. Perkins, and W. G. Scott, A redetermination of the neutrino mass squared difference in trimaximal mixing with terrestrial matter effects, Phys. Lett. B **458**, 79 (1999).

[6] E. Ma, A(4) symmetry and neutrinos with very different masses, Phys. Rev. D **70**, 031901 (2004).

[7] G. Altarelli and F. Feruglio, Tribimaximal neutrino mixing from discrete symmetry in extra dimensions, Nucl. Phys. **B720**, 64 (2005).
[8] G. Altarelli and F. Feruglio, Tribimaximal neutrino mixing, A(4) and the modular symmetry, Nucl. Phys. **B741**, 215 (2006).
[9] Y. Abe *et al.* (DOUBLE-CHOOZ Collaboration), Indication for the Disappearance of Reactor Electron Antineutrinos in the Double Chooz Experiment, Phys. Rev. Lett. **108**, 131801 (2012).
[10] F. P. An *et al.* (DAYA-BAY Collaboration), Observation of Electron-Antineutrino Disappearance at Daya Bay, Phys. Rev. Lett. **108**, 171803 (2012); Independent measurement of Theta13 via neutron capture on hydrogen at Daya Bay, Phys. Rev. D **90**, 071101 (2014).
[11] J. K. Ahn *et al.* (RENO Collaboration), Observation of Reactor Electron Antineutrino Disappearance in the RENO Experiment, Phys. Rev. Lett. **108**, 191802 (2012).
[12] K. Abe *et al.* (T2K Collaboration), Observation of Electron Neutrino Appearance in a Muon Neutrino Beam, Phys. Rev. Lett. **112**, 061802 (2014).
[13] B. Karmakar and A. Sil, Nonzero θ_{13} and leptogenesis in a type-I seesaw model with A_4 symmetry, Phys. Rev. D **91**, 013004 (2015).
[14] A. S. Joshipura and E. A. Paschos, Constraining leptogenesis from laboratory experiments, arXiv:hep-ph/9906498.
[15] A. S. Joshipura, E. A. Paschos, and W. Rodejohann, Leptogenesis in left-right symmetric theories, Nucl. Phys. **B611**, 227 (2001).
[16] B. Bajc, G. Senjanovic, and F. Vissani, b-tau Unification and Large Atmospheric Mixing: A Case for Noncanonical Seesaw, Phys. Rev. Lett. **90**, 051802 (2003).
[17] S. Antusch and S. F. King, From hierarchical to partially degenerate neutrinos via type-II upgrade of type-I seesaw models, Nucl. Phys. **B705**, 239 (2005).
[18] S. Antusch and S. F. King, Type-II leptogenesis and the neutrino mass scale, Phys. Lett. B **597**, 199 (2004).
[19] N. Sahu and S. U. Sankar, Bound on neutrino masses from leptogenesis in type-II seesaw models, Phys. Rev. D **71**, 013006 (2005).
[20] W. Rodejohann and Z. z. Xing, Flavor democracy and type-II seesaw realization of bilarge neutrino mixing, Phys. Lett. B **601**, 176 (2004).
[21] S. L. Chen, M. Frigerio, and E. Ma, Hybrid seesaw neutrino masses with A(4) family symmetry, Nucl. Phys. **B724**, 423 (2005).
[22] S. Bertolini and M. Malinsky, On *CP* violation in minimal renormalizable SUSY SO(10) and beyond, Phys. Rev. D **72**, 055021 (2005).
[23] E. K. Akhmedov and M. Frigerio, Interplay of type-I and type-II seesaw contributions to neutrino mass, J. High Energy Phys. 01 (2007) 043.
[24] W. Rodejohann, Type-II seesaw mechanism, deviations from bimaximal neutrino mixing and leptogenesis, Phys. Rev. D **70**, 073010 (2004).
[25] P. H. Gu, H. Zhang, and S. Zhou, A minimal type-II seesaw model, Phys. Rev. D **74**, 076002 (2006).
[26] A. Abada, P. Hosteins, F. X. Josse-Michaux, and S. Lavignac, Successful leptogenesis in SO(10) unification with a left-right symmetric seesaw mechanism, Nucl. Phys. **B809**, 183 (2009).
[27] D. Borah and M. K. Das, Neutrino masses and leptogenesis in type-I and type-II seesaw models, Phys. Rev. D **90**, 015006 (2014).
[28] D. Borah, Type-II seesaw origin of nonzero θ_{13}, δ_{CP} and leptogenesis, Int. J. Mod. Phys. A **29**, 1450108 (2014).
[29] M. Borah, D. Borah, M. K. Das, and S. Patra, Perturbations to $\mu - \tau$ symmetry, leptogenesis and lepton flavour violation with type-II seesaw, Phys. Rev. D **90**, 095020 (2014).
[30] R. Kalita, D. Borah, and M. K. Das, Corrections to scaling neutrino mixing: Nonzero θ_{13}, δ_{CP} and baryon asymmetry, Nucl. Phys. **B894**, 307 (2015).
[31] S. Pramanick and A. Raychaudhuri, An A4-based seesaw model for realistic neutrino mass and mixing, arXiv:1508.02330.
[32] M. Magg and C. Wetterich, Neutrino mass problem and gauge hierarchy, Phys. Lett. B **94**, 61 (1980).
[33] G. Lazarides, Q. Shafi, and C. Wetterich, Proton lifetime and fermion masses in an SO(10) model, Nucl. Phys. **B181**, 287 (1981).
[34] R. N. Mohapatra and G. Senjanovic, Neutrino masses and mixings in gauge models with spontaneous parity violation, Phys. Rev. D **23**, 165 (1981).
[35] J. Schechter and J. W. F. Valle, Neutrino masses in $SU(2) \times U(1)$ theories, Phys. Rev. D **22**, 2227 (1980).
[36] F. Capozzi, G. L. Fogli, E. Lisi, A. Marrone, D. Montanino, and A. Palazzo, Status of three-neutrino oscillation parameters, circa 2013, Phys. Rev. D **89**, 093018 (2014).
[37] M. C. Gonzalez-Garcia, M. Maltoni, and T. Schwetz, Updated fit to three neutrino mixing: Status of leptonic *CP* violation, J. High Energy Phys. 11 (2014) 052.
[38] D. V. Forero, M. Tortola, and J. W. F. Valle, Neutrino oscillations refitted, Phys. Rev. D **90**, 093006 (2014).
[39] T. D. Lee, A theory of spontaneous T violation, Phys. Rev. D **8**, 1226 (1973).
[40] A. E. Nelson, Naturally weak *CP* violation, Phys. Lett. B **136**, 387 (1984).
[41] S. M. Barr, Solving the Strong *CP* Problem Without the Peccei-Quinn Symmetry, Phys. Rev. Lett. **53**, 329 (1984).
[42] J. A. Harvey, P. Ramond, and D. B. Reiss, *CP* violation and mass relations in SO(10), Phys. Lett. B **92**, 309 (1980).
[43] J. A. Harvey, D. B. Reiss, and P. Ramond, Mass relations and neutrino oscillations in an SO(10) model, Nucl. Phys. **B199**, 223 (1982).
[44] G. C. Branco, Spontaneous *CP* nonconservation and natural flavor conservation: A minimal model, Phys. Rev. D **22**, 2901 (1980).
[45] L. Bento and G. C. Branco, Generation of a K-M phase from spontaneous *CP* breaking at a high-energy scale, Phys. Lett. B **245**, 599 (1990).
[46] L. Bento, G. C. Branco, and P. A. Parada, A minimal model with natural suppression of strong *CP* violation, Phys. Lett. B **267**, 95 (1991).
[47] G. C. Branco, P. A. Parada, and M. N. Rebelo, A common origin for all *CP* violations, arXiv:hep-ph/0307119.
[48] G. C. Branco, R. Gonzalez Felipe, F. R. Joaquim, and H. Serodio, Spontaneous leptonic *CP* violation and nonzero θ_{13}, Phys. Rev. D **86**, 076008 (2012).

[49] G. C. Branco, T. Morozumi, B. M. Nobre, and M. N. Rebelo, A bridge between CP violation at low-energies and leptogenesis, Nucl. Phys. **B617**, 475 (2001).

[50] T. Araki and H. Ishida, Partial mass-degeneracy and spontaneous CP violation in the lepton sector, Prog. Theor. Exp. Phys. **2014**, 013B01 (2014).

[51] Y. H. Ahn, S. K. Kang, and C. S. Kim, Spontaneous CP violation in A_4 flavor symmetry and leptogenesis, Phys. Rev. D **87**, 113012 (2013).

[52] J. E. Kim and S. Nam, Unifying CP violations of quark and lepton sectors, arXiv:1506.08491.

[53] S. F. Ge, H. J. He, and F. R. Yin, Common origin of soft mu-tau and CP breaking in neutrino seesaw and the origin of matter, J. Cosmol. Astropart. Phys. 05 (2010) 017.

[54] H. J. He and F. R. Yin, Common origin of $\mu-\tau$ and CP breaking in neutrino seesaw, baryon asymmetry, and hidden flavor symmetry, Phys. Rev. D **84**, 033009 (2011).

[55] A. E. C. Hernndez and R. Martinez, Fermion mass and mixing pattern in a minimal T7 flavor 331 model, arXiv:1501.07261.

[56] Y. Achiman, Can one phase induce all CP violations including leptogenesis?, Phys. Lett. B **599**, 75 (2004).

[57] Y. Achiman, Spontaneous CP violation in SUSY SO(10), Phys. Lett. B **653**, 325 (2007).

[58] M. D. Campos, A. E. C. Hernndez, H. Ps, and E. Schumacher, Higgs $\to \mu\tau$ as an indication for S_4 flavor symmetry, Phys. Rev. D **91**, 116011 (2015).

[59] A. E. Crcamo Hernndez and R. Martinez, Lepton masses and mixings in a 331 model with A_4 flavour symmetry, arXiv:1501.05937.

[60] C. Arbelez, A. E. C. Hernndez, S. Kovalenko, and I. Schmidt, Adjoint $SU(5)$ GUT model with T_7 flavor symmetry, arXiv:1507.03852.

[61] M. Frank, Leptogenesis in the left-right supersymmetric model, Phys. Rev. D **70**, 036004 (2004).

[62] M. C. Chen and K. T. Mahanthappa, Relating leptogenesis to low energy flavor violating observables in models with spontaneous CP violation, Phys. Rev. D **71**, 035001 (2005).

[63] N. Sahu and S. U. Sankar, Heavy neutrino mass hierarchy from leptogenesis in left-right symmetric models with spontaneous CP-violation, Nucl. Phys. **B724**, 329 (2005).

[64] W. Chao, S. Luo, and Z. z. Xing, Neutrino mixing and leptogenesis in type-II seesaw scenarios with left-right symmetry, Phys. Lett. B **659**, 281 (2008).

[65] K. A. Olive *et al.* (Particle Data Group Collaboration), Review of particle physics, Chin. Phys. C **38**, 090001 (2014).

[66] S. Fukuda *et al.* (Super-Kamiokande Collaboration), Determination of solar neutrino oscillation parameters using 1496 days of Super-Kamiokande I data, Phys. Lett. B **539**, 179 (2002); Y. Ashie *et al.* (Super-Kamiokande Collaboration), A measurement of atmospheric neutrino oscillation parameters by SUPER-KAMIOKANDE I, Phys. Rev. D **71**, 112005 (2005); P. Adamson *et al.* (MINOS Collaboration), Measurement of the Neutrino Mass Splitting and Flavor Mixing by MINOS, Phys. Rev. Lett. **106**, 181801 (2011); T. Araki *et al.* (KamLAND Collaboration), Measurement of Neutrino Oscillation with KamLAND: Evidence of Spectral Distortion, Phys. Rev. Lett. **94**, 081801 (2005).

[67] P. A. R. Ade *et al.* (Planck Collaboration), Planck 2013 results. XVI. Cosmological parameters, Astron. Astrophys. **571**, A16 (2014).

[68] K. Asakura *et al.* (KamLAND-Zen Collaboration), Results from KamLAND-Zen, AIP Conf. Proc. **1666**, 170003 (2015).

[69] J. B. Albert *et al.* (EXO-200 Collaboration), Search for Majorana neutrinos with the first two years of EXO-200 data, Nature (London) **510**, 229 (2014).

[70] S. F. King and C. Luhn, Trimaximal neutrino mixing from vacuum alignment in A4 and S4 models, J. High Energy Phys. 09 (2011) 042.

[71] G. Altarelli, F. Feruglio, and L. Merlo, Tribimaximal neutrino mixing and discrete flavour symmetries, Fortschr. Phys. **61**, 507 (2013).

[72] For a review, see S. Davidson, E. Nardi, and Y. Nir, Leptogenesis, Phys. Rep. **466**, 105 (2008), and references therein.

[73] P. J. O'Donnell and U. Sarkar, Baryogenesis via lepton number violating scalar interactions, Phys. Rev. D **49**, 2118 (1994).

[74] E. Ma and U. Sarkar, Neutrino Masses and Leptogenesis with Heavy Higgs Triplets, Phys. Rev. Lett. **80**, 5716 (1998).

[75] T. Hambye, E. Ma, and U. Sarkar, Supersymmetric triplet Higgs model of neutrino masses and leptogenesis, Nucl. Phys. **B602**, 23 (2001).

[76] T. Hambye, M. Raidal, and A. Strumia, Efficiency and maximal CP-asymmetry of scalar triplet leptogenesis, Phys. Lett. B **632**, 667 (2006).

[77] G. C. Branco, R. G. Felipe, and F. R. Joaquim, Leptonic CP violation, Rev. Mod. Phys. **84**, 515 (2012).

[78] D. A. Sierra, F. Bazzocchi, I. de Medeiros Varzielas, L. Merlo, and S. Morisi, Tribimaximal lepton mixing and leptogenesis, Nucl. Phys. **B827**, 34 (2010).

[79] D. A. Sierra and I. de Medeiros Varzielas, The role of lepton flavor symmetries in leptogenesis, Fortschr. Phys. **61**, 645 (2013).

[80] T. Hambye and G. Senjanovic, Consequences of triplet seesaw for leptogenesis, Phys. Lett. B **582**, 73 (2004).

[81] S. Antusch, Flavour-dependent type-II leptogenesis, Phys. Rev. D **76**, 023512 (2007).

[82] E. K. Akhmedov and W. Rodejohann, A Yukawa coupling parametrization for type-$I+II$ seesaw formula and applications to lepton flavor violation and leptogenesis, J. High Energy Phys. 06 (2008) 106.

[83] D. Aristizabal Sierra, F. Bazzocchi, and I. de Medeiros Varzielas, Leptogenesis in flavor models with type-I and II seesaws, Nucl. Phys. **B858**, 196 (2012).

[84] T. Hambye, Leptogenesis: Beyond the minimal type-I seesaw scenario, New J. Phys. **14**, 125014 (2012).

[85] D. A. Sierra, M. Dhen, and T. Hambye, Scalar triplet flavored leptogenesis: A systematic approach, J. Cosmol. Astropart. Phys. 08 (2014) 003.

[86] G. Lazarides and Q. Shafi, R symmetry in minimal supersymmetry standard model and beyond with several consequences, Phys. Rev. D **58**, 071702 (1998).

[87] J. N. Fry, K. A. Olive, and M. S. Turner, Higgs bosons and the evolution of baryon asymmetries, Phys. Rev. D **22**, 2977 (1980).

[88] E. Ma, S. Sarkar, and U. Sarkar, Scale of SU(2)(R) symmetry breaking and leptogenesis, Phys. Lett. B **458**, 73 (1999).

[89] T. Hambye, Various realizations of leptogenesis and neutrino mass constraints, arXiv:hep-ph/0412053.

[90] T. Hambye, Y. Lin, A. Notari, M. Papucci, and A. Strumia, Constraints on neutrino masses from leptogenesis models, Nucl. Phys. **B695**, 169 (2004).

[91] S. Lavignac and B. Schmauch, Flavour always matters in scalar triplet leptogenesis, J. High Energy Phys. 05 (2015) 124.